UNIVERSITY OF CALIFORNIA, SAN DIEGO

Stability Properties of Self-Propelled Wakes

A thesis submitted in partial satisfaction of the
requirements for the degree
Master of Science

in

Engineering Sciences (Aerospace Engineering)

by

Tej Patel

Committee in charge:

Professor Eric Lauga, Chair
Professor Alison Marsden
Professor Sutanu Sarkar

2012

The thesis of Tej Patel is approved, and it is acceptable in quality and form for publication on microfilm and electronically:

_____

_____

_____

Chair

University of California, San Diego

2012

DEDICATION

To my grandfather, Manu Patel.

EPIGRAPH

Scientists discover the world that exists,
engineers create the world that never was.
—Theodore Von Kármán

TABLE OF CONTENTS

LIST OF FIGURES

ACKNOWLEDGEMENTS

There is not one, or few, people that I can thank for making this thesis come to fruition. Obviously my parents and my wonderful fiancée are to be thanked for all of the support through late nights and production of copious amounts of coffee. I must also thank both my advisors, Prof. Lauga and Prof. Eloy, who helped me an enormous amount and were extremely understanding of my situation.

Finally, I want to thank all of my friends who, through these arduous times, still remain my friends. I know I disappeared for 2 years, but I promise I'll be back soon!

VITA

2010	B. S. in Aerospace Engineering, University of California, San Diego
2010	B. A. in Applied Mathematics, University of California, San Diego
2010-2012	Design and Development Engineer, MagCanica, Inc.
2012	M. S. in Aerospace Engineering, University of California, San Diego

PUBLICATIONS

R. Kari, T. Patel, S. Bitar, B. Canilang, and A. Bonafede. "Magnetoelastic Torquemeter System for LCAC Hovercraft Turboshaft Engine Monitoring and Control", *ASME Turbo Expo*, In Proc., 2012.

J.C. Bebel, N. Howard, and T. Patel. "An autonomous system used in the DARPA Grand Challenge", *The 7th International IEEE Conference on Intelligent Transportation Systems*, In Proc., 2004.

ABSTRACT OF THE THESIS

Stability Properties of Self-Propelled Wakes

by

Tej Patel

Master of Science in Engineering Sciences (Aerospace Engineering)

University of California, San Diego, 2012

Professor Eric Lauga, Chair

This thesis focuses on the stability characteristics of a momentum-less wake. Momentum-less wakes are wakes produced by self-propelled bodies and can be found in any numerous fluid flows, such as the flow behind a submarine, or fish. In this thesis we try to relate the momentum-less wake described to a wake behind a fish through specific choices in non-dimensional terms. We then look at both the temporal and spatial stability characteristics. While the temporal stability characteristics appeared to give results of interest, it appeared that the spatial stability characteristics were not as interesting.

This thesis also goes into detail about two popular numerical methods of solving the Orr-Sommerfeld equation, and how to use these methods on the less common unbounded domain type flows.

Chapter 1

Introduction

Hydrodynamic stability is an important topic in fluid mechanics that became of great interest in the early part of the 19th century. The primary goal of hydrodynamic stability is in understanding whether a laminar flow, when perturbed, will transition to some new state. In a very general sense, it is understood that a flow which is perturbed and returns to its original state is stable, while a flow which comes to a new state is considered unstable. The study of hydrodynamic stability has many practical applications in engineering such as calculations of aerodynamic drag, or nuclear power-plant heat exchangers. Within hydrodynamic stability there are many different sub-topics related to the different forms of hydrodynamic stability, such as stability of flows caused by convection, or stability of parallel shear flows. This thesis will focus on the stability of parallel shear flows related to wakes self-propelled objects.

1.1 Disturbance Equations

As with any fluid flow, the study of stability starts with the Navier-Stokes Equations. In particular, we wish to rewrite the Navier-Stokes equation in a form that we may use to study the effect of a velocity or pressure perturbation on a

base flow. The Navier-Stokes equations appear as

$$\frac{\partial \mathbf{u}}{\partial t} + \mathbf{u} \cdot \nabla \mathbf{u} = -\nabla p + \frac{1}{\mathrm{Re}} \nabla^2 \mathbf{u} \tag{1.1}$$

$$\nabla \mathbf{u} = 0 \tag{1.2}$$

To derive the disturbance equations, assume that we have some base flow, $\mathbf{U}$ with velocity components U, V, and W which satisfies the Navier-Stokes equation, and there exists a perturbation on top of this flow as follows,

$$u = U(x, y, t) + \tilde{u}(x, y, t) \tag{1.3}$$

$$v = V(x, y, t) + \tilde{v}(x, y, t) \tag{1.4}$$

$$z = W(x, y, t) + \tilde{w}(x, y, t) \tag{1.5}$$

$$p = P(x, y, t) + \tilde{p}(x, y, t) \tag{1.6}$$

Here, u, v, and w, are the x, y, and z components of the fluid velocity, while the components, $\tilde{u}$, $\tilde{v}$, and $\tilde{w}$ denote the perturbation velocities. In vector form this reads,

$$\mathbf{u} = \mathbf{U} + \tilde{\mathbf{u}} \tag{1.7}$$

$$p = P + \tilde{p} \tag{1.8}$$

We assume that $\mathbf{U}$, $\tilde{\mathbf{u}}$, P, and $\tilde{p}$ satisfy the Navier-Stokes equations, so we input (1.7) and (1.8) into equation (1.1). This results in the following,

$$\frac{\partial \mathbf{U}}{\partial t} + \frac{\partial \tilde{\mathbf{u}}}{\partial t} + \mathbf{U} \cdot \nabla \tilde{\mathbf{u}} + \tilde{\mathbf{u}} \cdot \nabla \tilde{\mathbf{u}} + \mathbf{U} \cdot \nabla \mathbf{U} + \tilde{\mathbf{u}} \cdot \nabla \mathbf{U} = - \nabla P - \nabla \tilde{p} + \frac{1}{\mathrm{Re}} \nabla U + \frac{1}{\mathrm{Re}} \nabla \tilde{u} \tag{1.9}$$

Taking the above equations, and subtracting the mean flow state, we arrive at the non-linear disturbance equation,

$$\frac{\partial \tilde{\mathbf{u}}}{\partial t} + \mathbf{U} \cdot \nabla \tilde{\mathbf{u}} + \tilde{\mathbf{u}} \cdot \nabla \tilde{\mathbf{u}} + \tilde{\mathbf{u}} \cdot \nabla \mathbf{U} = -\nabla \tilde{p} + \frac{1}{\mathrm{Re}} \nabla \tilde{u} \tag{1.10}$$

$$\nabla \cdot \tilde{\mathbf{u}} = 0 \tag{1.11}$$

Equation (1.10) and (1.11) now represent the non-linear disturbance equations. Because we assume the perturbed quantities, $\tilde{\mathbf{u}}$ and $\tilde{p}$ to be small, we can linearize

(1.10) by ignoring the products of small quantities yielding the following:

$$\frac{\partial \tilde{\mathbf{u}}}{\partial t} + \mathbf{U} \cdot \nabla \tilde{\mathbf{u}} + \tilde{\mathbf{u}} \cdot \nabla \mathbf{U} = -\nabla \tilde{\mathbf{p}} + \frac{\mathbf{1}}{\mathrm{Re}} \nabla \tilde{\mathbf{u}} \tag{1.12}$$

The derived disturbances equations can now be used to derive both the Orr-Sommerfeld equation and the Rayleigh equation.

1.2 Definition of Stability

Roughly speaking, a flow is assumed to be stable if for all time, the perturbations to a base flow, $\tilde{\mathbf{u}}$ and $\tilde{p}$, do not grow. There can be multiple ways of defining the growth of a perturbation [6], but a common metric is to define the energy of a perturbation. Following [18], if we take the energy of the perturbed flow to be given as,

$$E_v = \frac{1}{2} \int_V \tilde{\mathbf{u}} \tilde{\mathbf{u}} dV \tag{1.13}$$

Then we can say that a flow is stable to a perturbation if

$$\lim_{t \to \infty} \frac{E_v(t)}{E_v(0)} \to 0. \tag{1.14}$$

1.3 Temporal and Spatial Stability

The study of stability for fluid flows can be broken into two primary classes of stability, temporal stability, and spatial stability. Temporal stability focuses on the amplitude or energy increase of a perturbation in time, we ask the question: does a point source perturbation die out or increase in strength? Spatial stability however focuses on how a perturbation behaves in time and space. The primary questions to ask in spatial stability problems is, does the perturbation die out? Does it get advected from the original point source? Does it spread both forward and backward in space? The last point of whether a perturbation will move forward and backward of its point source in space is known as a absolute instability.

1.4 Thesis Outline

The first chapter of this thesis focuses on the background of stability calculations, and goes over the basic concepts of stability. The second chapter will focus on the derivation of the Rayleigh, and Orr-Sommerfeld equations which are the basic equations for stability analysis. Chapter two will also cover basic solutions to both of these equations for the temporal and spatial stability cases. Chapter three will cover the numerical methods used for the this research, in particular there will be a comparison of both the finite difference, and Chebyshev collocation methods. Chapter four will then focus on the temporal and spatial stability of wakes behind self propelled or towed objects. This will include the derivation of the velocity profile of a wake behind a self-propelled body, as well as the results for the stability calculations. Finally chapter five will conclude with possible future work, including the possibility of using more modern techniques for stability calculations.

Chapter 2

Background

For both the derivation of inviscid and viscous flow stability problems, we assume a flow profile that varies only in the y direction and is constant in both the x and z directions, as is shown in Figure 2.1. In Figure 2.1, the fluid velocity in the x direction is given by u, while the y and z components of velocity are given by v and w respectively.

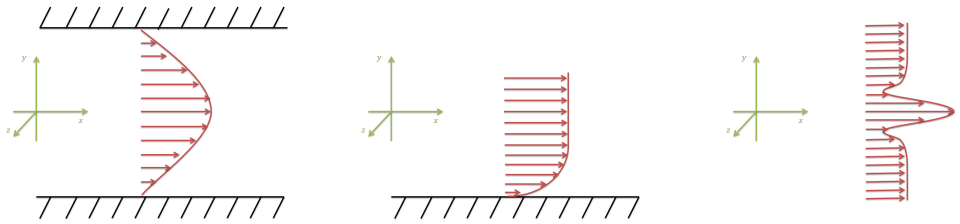

(a) Channel flow (b) Boundary layer flow (c) Jet / Wake flow

Figure 2.1: Parallel flow schematics showing coordinate systems

2.1 Inviscid Stability: The Rayleigh Equation

The derivation of the Rayleigh equation, following [18], begins with the simplification of the disturbance equations (1.10). By assuming an inviscid fluid with flow profiles similar to Figure 2.1 (mainly the base flow, U is only a function of y), then we can simplify the linear disturbance equations, (1.10) and (1.11) into

the following form:

$$\frac{\partial u}{\partial t} + U\frac{\partial u}{\partial x} + v\frac{\mathrm{d}U}{\mathrm{d}y} = -\frac{\partial p}{\partial x} \tag{2.1}$$

$$\frac{\partial v}{\partial t} + U\frac{\partial v}{\partial x} = -\frac{\partial p}{\partial y} \tag{2.2}$$

$$\frac{\partial w}{\partial t} + U\frac{\partial w}{\partial x} = -\frac{\partial p}{\partial z} \tag{2.3}$$

along with the continuity equation

$$\frac{\partial u}{\partial x} + \frac{\partial v}{\partial y} + \frac{\partial w}{\partial z} \tag{2.4}$$

By taking the divergence of (2.1) through (2.3), and combining with the continuity equation, an equation for the perturbation pressure is obtained which can then be used with equation (2.2) to remove the pressure term altogether, leaving the following equation

$$\left[\left(\frac{\partial}{\partial t} + U\frac{\partial}{\partial x}\right)\nabla^2 - U''\frac{\partial}{\partial x}\right]v = 0 \tag{2.5}$$

Here we take the prime to mean that we have taken a derivative with respect to the y direction. Now, we assume wavelike perturbations of the form

$$v(x, y, z, t) = \phi e^{i(\alpha x + \beta z - \alpha c t)} \tag{2.6}$$

Here, α is the stream-wise wave number and β is the span-wise wave number, and αc is the complex frequency, ω. Because in this research we are only looking at two dimensional flows, the span-wise wave number, β will be assumed to be zero, this yields the following,

$$v(x, y, z, t) = \phi e^{i(\alpha x - \alpha c t)} \tag{2.7}$$

In the case of temporal stability for fluid flows, c is the eigenvalue to the problem, and is thought of as the complex phase speed of the perturbation. The perturbation amplitude will grow or decay in time like $e^{c_i t}$. Thus, a flow is stable if $c_i < 0$, and unstable otherwise. Now, if we input equation (2.7) into (2.5), we get the following,

$$\begin{aligned} &i\alpha^3 c\phi e^{i(\alpha x - \alpha c t)} - i\alpha c\phi'' e^{i(\alpha x - \alpha c t)} + i\alpha U\phi'' e^{i(\alpha x - \alpha c t)} \\ &- i\alpha^3 U\phi e^{i(\alpha x - \alpha c t)} - i\alpha U''\phi e^{i(\alpha x - \alpha c t)} = 0 \end{aligned} \tag{2.8}$$

dividing equation (2.8) by $i\alpha e^{i(\alpha x-\alpha ct)}$ and simplifying, we can arrive at the Rayleigh stability equation.

$$(U-c)(\phi-k^2\phi)-U''\phi=0 \tag{2.9}$$

The boundary conditions for this problem are as follows,

$$\phi(\partial\Omega)=0 \tag{2.10}$$

for bounded flows, and

$$\phi(\pm\infty) \quad \text{bounded} \tag{2.11}$$

for unbounded flows. Equation (2.9) along with its corresponding boundary conditions now makes an eigenvalue problem to determine stability of a base flow U. As stated before, for the temporal case the eigenvalue is c, and is complex, while the wave number, α is real and supplied. However, if we wish to study the case of spatial instabilities, the eigenvalue becomes α and α is allowed to be complex, while the frequency ω (and consequently c) is real and supplied.

2.2 Viscous Stability: The Orr-Sommerfeld Equation

2.2.1 Derivation

The derivation of the Orr-Sommerfeld closely follows the derivation of the Rayleigh equation, so following in [18], we start with the linear disturbance equations (1.10) and (1.11), assuming a fully developed base flow, U which varies only in the y direction, as shown in Figure 2.1. Keeping the viscous terms, and ignoring the non-linear terms we have the following set of equations,

$$\frac{\partial u}{\partial t}+U\frac{\partial u}{\partial x}+vU'=-\frac{\partial p}{\partial x}+\frac{1}{\mathrm{Re}}\nabla^2 u \tag{2.12}$$

$$\frac{\partial v}{\partial t}+U\frac{\partial v}{\partial x}=-\frac{\partial p}{\partial y}+\frac{1}{\mathrm{Re}}\nabla^2 v \tag{2.13}$$

$$\frac{\partial w}{\partial t}+U\frac{\partial w}{\partial x}=-\frac{\partial p}{\partial z}+\frac{1}{\mathrm{Re}}\nabla^2 w \tag{2.14}$$

and the continuity equation,

$$\frac{\partial u}{\partial x} + \frac{\partial v}{\partial y} + \frac{\partial w}{\partial z} = 0 \tag{2.15}$$

In these equations, as before, U' and U'' refer to the the first and second derivatives of U with respect to y. If we now take the divergence of equations (2.12), (2.13), and (2.14), and then use equation (2.15) to simplify, we arrive at the following equation for the perturbation pressure very much like how we did during the derivation of the Rayleigh equation.

$$\nabla^2 p = -2U' \frac{\partial v}{\partial x} \tag{2.16}$$

Combining the above equation with equation (2.13) we now arrive at the equation for the normal velocity

$$\left[\left(\frac{\partial}{\partial t} + U \frac{\partial}{\partial x} \right) \nabla^2 - U'' \frac{\partial}{\partial x} - \frac{1}{\mathrm{Re}} \nabla^4 \right] \phi = 0 \tag{2.17}$$

Now, as we did for the Rayleigh equation, we assume that we have wavelike perturbation as shown in equation (2.7). If we input these perturbations into equation (2.17), and simplify we can arrive at the following equation

$$(U - c)(\phi'' - \alpha^2 \phi) i - U'' \phi - \frac{1}{i\alpha \mathrm{Re}} (\phi^{\mathrm{iv}} - 2\alpha^2 \phi'' + \alpha^4 \phi) = 0, \tag{2.18}$$

which is the classical Orr-Sommerfeld equation. Again, like the Rayleigh equation, c is known as the complex wave speed and is the eigenvalue for the problem. α and the Reynold's number, Re, are parameters which are supplied in the case of the temporal stability problem. Because the Orr-Sommerfeld equation is a 4th order ODE, we require four boundary conditions in order to uniquely solve the problem. The boundary conditions for bounded flows are given as,

$$\phi(\partial\Omega) = \phi'(\partial\Omega) = 0 \tag{2.19}$$

and for unbounded flows, and

$$\phi(\pm\infty)\text{bounded} \tag{2.20}$$

As can be seen in equation (2.18), if we take the Reynolds number to the limit, $\mathrm{Re} \to \infty$, we can see that we will receive back the Rayleigh equation, which is simply the Orr-Sommerfeld equation at the inviscid limit.

2.2.2 Applications of the Orr-Sommerfeld Equation - Temporal Stability of Plane Poiseuille Flow

The Orr-Sommerfeld equation along with its associated boundary conditions defines a eigenvalue problem from which we can determine if a given base flow is stable to sinusoidal perturbations. In the case of temporal stability, the Reynolds number Re and wave number α are given as parameters, while the eigenvalue, ω needs to be determined. In this case α is to be real while ω can be complex. In the case of spatial stability, instead of α being a parameter, the frequency ω is the parameter along with the Reynolds number. The wave number, α is then allowed to be complex.

One classical application of solving the Orr-Sommerfeld equation is for the case of plane Poiseuille flow where we have a flow defined on the interval, $-1 < y < 1$. The objective is to determine the stability characteristics of plane Poiseuille flow for various Reynolds numbers and wave numbers. For plane Poiseuille flow, we know that the base flow is given in non-dimensional terms as follows

$$U(y) = 1 - y^2 \tag{2.21}$$

If we now use this baseflow in the Orr-Sommerfeld equation, (2.18), we can solve for the eigenvalue spectra to determine when the flow is stable or unstable. The problem to solve is as follows,

$$0 = (U - c)(\mathcal{D}^2 - k^2)\phi - U''\phi - \frac{1}{i\alpha \mathrm{Re}}(\mathcal{D}^2 - k^2)^2\phi \tag{2.22}$$

$$U(y) = 1 - y^2 \tag{2.23}$$

$$0 = \phi(\pm 1) = \phi'(\pm 1) \tag{2.24}$$

This problem is not trivial, and cannot be solved in a closed form analytical method, thus numerical methods need to be used. There are a number of numerical methods available to solve this problem as will be discussed in Chapter 3. For now we will simply look at the solutions to these example problems.

If we look at the case of plane Poiseuille flow with a Reynolds number of $\mathrm{Re} = 2,000$, and a wave number, $\alpha = 1$, we obtain the eigenvalue spectra shown in

Figure 2.2. As can be seen in Figure 2.2, all of the eigenvalues have an imaginary part that is negative, thus implying that the base flow is stable for perturbations of wave number $\alpha = 1$ at a Reynolds number of 2,000. If, however, we look at Figure 2.3, where the Reynolds number is 7,000 and $\alpha = 1.02$, we will see that the flow is no longer stable. In Figure 2.3, we see that there exists one eigenvalue that has an imaginary part larger than zero, thus causing instabilities.

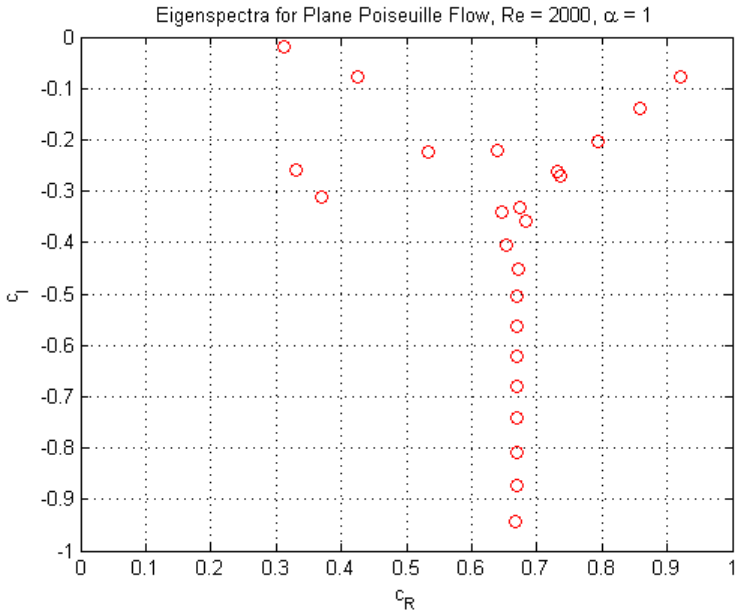

Figure 2.2: Plot of the eigenvalues, c of plane Poiseuille flow for Re = 2000 and $\alpha = 1$. Notice the three distinct branches of the eigenvalues.

It is interesting to note also the different branches that exist in the eigenvalue spectrum. Specifically, we can see the vertical branch of eigenvalues, known as the continuous spectrum of the Orr-Sommerfeld equation, and the two branches coming off the vertical branch at an angle. These angled branches are known as the discrete spectrum of the Orr-Sommerfeld equation. As it turns out, flows which are bounded, like Poiseuille flow have an infinite many number of eigenvalues in the discrete spectrum. However, as was shown by [16], it turns out that flows on unbounded domains have only finitely many eigenvalues in the discrete spectrum.

It is clear that a flow's stability characteristics depend on the parameters, α and Re, so it is natural to ask on for what values of the parameters is a given

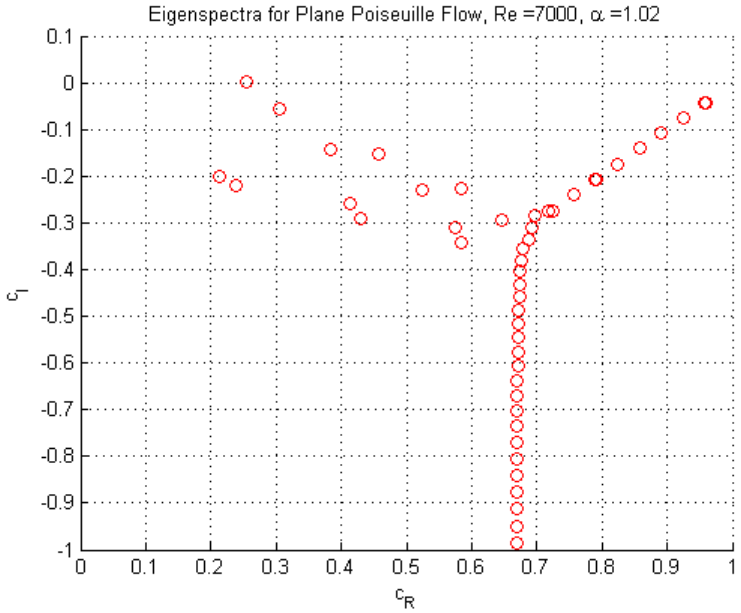

Figure 2.3: Plot of the eigenvalues, c of plane Poiseuille flow for Re $= 7000$ and $\alpha = 1.02$.

flow stable or unstable. To determine this, we look at the marginal stability curve a flow. The marginal stability curve shows the curve in the α-Re plane, where the largest imaginary part of the eigenvalues from the Orr-Sommerfeld equation are equal to zero. Hence the marginal curve shows the transition point from stable to unstable flows. The marginal curve for the example of plane Poiseuille flow is given is Figure 2.4.

2.3 Spatial Stability

In temporal stability, we wish to look at how the amplitude of a perturbation changes for a given base flow over time, but in the case of spatial stability we wish to study how the frequency of the overall structure of the spatial and temporal stability problem is the same in the sense that the Orr-Sommerfeld or Rayleigh equation is still the governing equation. The difficulty arises in how the eigenvalues which we are looking for are no longer linear in the Orr-Sommerfeld or Rayleigh equation, but rather show up as a polynomials.

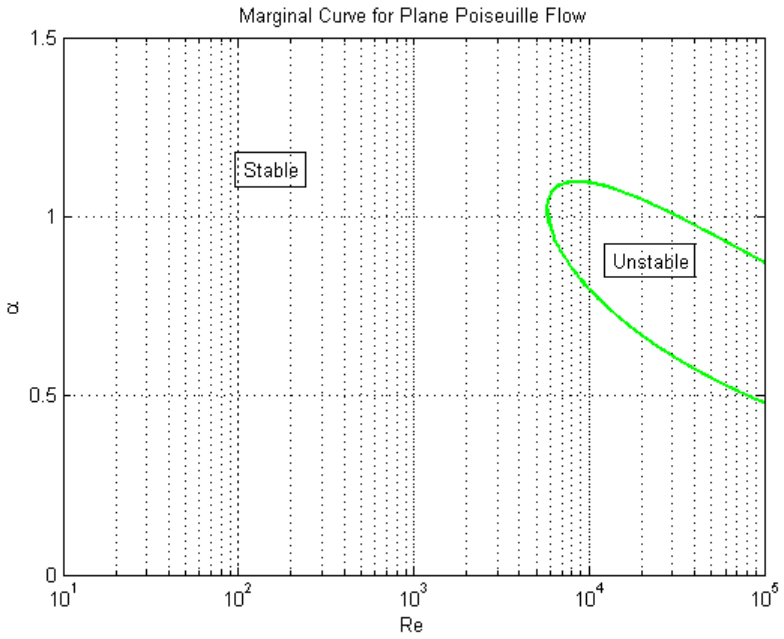

Figure 2.4: Plot of the marginal curve for plane Poiseuille. The critical values of α and Re (the 'nose' of the curve) are, $\alpha_c = 1.02$ and $\mathrm{Re}_c = 5,772$.

2.3.1 Absolute and Convective Instabilities

As was discussed earlier, in spatial stability analysis, one wants to understand if a given base flow will have an absolute or convective instability. We can think of an absolute instability as a flow which will grow in both space and time as in Figure 2.5. In Figure 2.5 we can see how the disturbance, which originates from the origin, is propagating forward in time, but also in all directions of space. Eventually, as time progress, this disturbance will affect the entire fluid. A convective instability however behaves differently, in the sense that the disturbance is advected away from its originating point, and will only ever affect a local area of the fluid. Figure 2.6 shows a convectively stable flow.

In order to determine if a flow is absolutely or convectivly unstable, we first bring up the idea of a dispersion relation which is a complex function that relates the wave number α, and frequency ω. Mathematically, the dispersion relation is given as

$$D(\alpha, \omega) = 0 \tag{2.25}$$

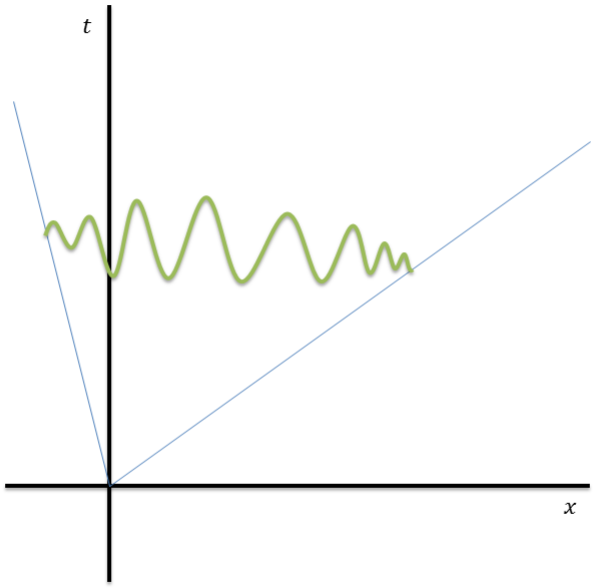

Figure 2.5: Schematic plot of an absolute instability. The disturbance (green) originates from the origin and propagates in time and space. Notice the disturbance moves both forward and backward in space.

The dispersion relationship for parallel shear flows can be obtained by finding the solution of the Orr-Sommerfeld equation, as solving the eigenvalue problem for either ω (the temporal branch of the dispersion relation), or α (the spatial branch) creates a relation between the two values. Using this dispersion relationship, we can study a flow's response to an impulse in both space and time.

An absolute instability will occur in a flow if there exists a branch point in the ω plane that is above the ω_R axis. If a branch point does exist in the complex ω plane, by virtue of coupling through the dispersion relationship, a type of saddle point known as a pinch point will form in the α plane. The mathematical framework behind spatial instabilities is fairly convoluted, so a brief outline is presented following, [18]

To model a flows response to a impulse, it is helpful to begin by defining a

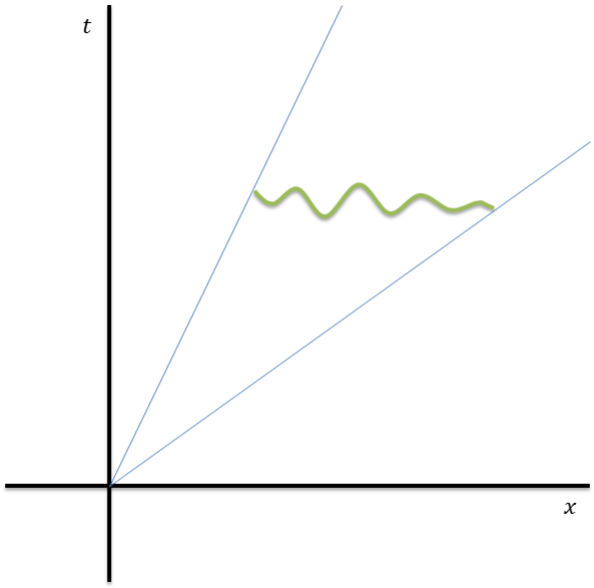

Figure 2.6: Schematic plot of convective instability. The disturbance (green) originates from the origin and propagates in time and space. Notice however that the disturbance only moves backwards in space.

Green's function $G(x,t)$ which abides by the following relationship,

$$D\left(-i\frac{\partial}{\partial x}, i\frac{\partial}{\partial t}\right) G(x,t) = \delta(x)\delta(t). \tag{2.26}$$

Now we can mathematically define a convective instability as a flow that has the following properties,

$$\lim_{t\to\infty} G(x,t) \to \infty \qquad \text{for at least one ray} \frac{x}{t} = \text{constant} \tag{2.27}$$

$$\lim_{t\to\infty} G(x,t) = 0 \qquad \text{for the ray} \frac{x}{t} = 0 \tag{2.28}$$

similarly, an absolute instability can be defined as follows,

$$\lim_{t\to\infty} G(x,t) \to \infty \qquad \text{for at least one ray} \frac{x}{t} = \text{constant} \tag{2.29}$$

$$\lim_{t\to\infty} G(x,t) \to \infty \qquad \text{for the ray} \frac{x}{t} = 0 \tag{2.30}$$

The Green's function $G(x,t)$ is found by taking the Fourier and Laplace transform of equation (2.26). We take the Fourier transform in the α variable, and Laplace transform in the ω variable. Doing this yields the following,

$$G(x,t) = \frac{1}{4\pi}\int_L\int_F \frac{e^{i(\alpha x-\omega t)}}{D(\alpha,\omega)} \quad \mathrm{d}\alpha\mathrm{d}\omega. \tag{2.31}$$

Here L represents the counter integration path in the ω plane, while F represents the counter integration path in the α plane. If we now follow the method introduced by Briggs, [18], we can determine if a singularity that exists which causes an absolute or convective instability. We first rewrite equation (2.31) as follows

$$G(x,t) = \frac{1}{2\pi}\int_L e^{-i\omega t}\left[\frac{1}{2\pi}\int_F \frac{e^{i\alpha x}}{D(\alpha,\omega)}\mathrm{d}\alpha\right]\mathrm{d}\omega. \tag{2.32}$$

Generally speaking, the goal is to lower the Laplace contour, L, to below the ω_R line using analytic continuation. If a singularity exists, this will not be possible, and a cusp in complex ω plane will form. Because doing this procedure analytically is incredibly difficult for even the most basic flows due to the inherent complexity of the dispersion relations, a fairly simple numerical approach to determining the locations of singularities in the complex ω plane exist.

2.3.2 Cusp Map Method

Because it is much easier mathematically to solve the temporal stability problem, a method to relate the spatial and temporal stability problems is highly desirable. The goal would be that one can solve the temporal stability case and retrieve the spatial stability characteristics of a flow. As it so turns out, the cusp map method allows one to do exactly this.

The idea behind the cusp map method is to map lines of constant α_I in the complex α plane, to the complex ω plane using the Orr-Sommerfeld equation. If there is an absolute or convective instability, we will see it as a cusp forming in the ω plane as shown in Figure 2.7. If the cusp forms above the ω_R axis, then we know that a absolute instability has formed, while if the cusp forms below the ω_R axis, then a convective instability exists in the flow. In order to determine

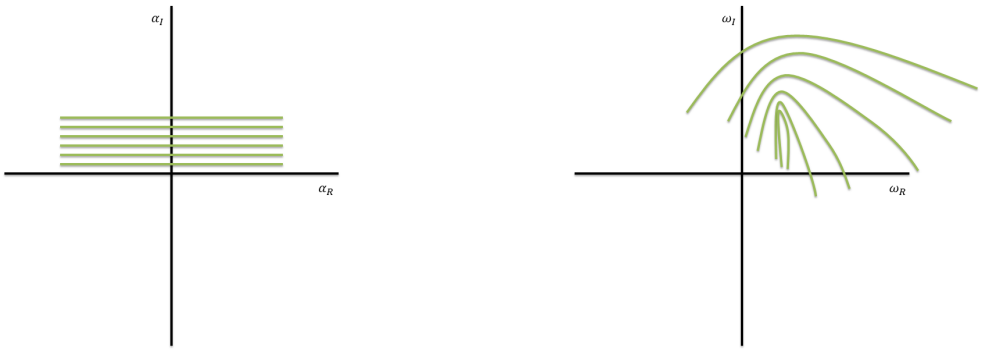

(a) Lines of α_I = Constant (b) α mapped to the complex ω plane

Figure 2.7: Schematic drawing of the cusp map method. The grid in the complex α plane 2.7a gets mapped via the dispersion relationship (solving the temporal Orr-Sommerfeld Equation) to the complex ω plane. A singularity exists where the tip of the cusp is forming in the ω plane.

the mapping from the complex α to complex ω plane, we need to solve the Orr-Sommerfeld equation. By solving the Orr-Sommefeld equation for a complex α, we obtain the eigenvalues, ω, of which we pick the most unstable eigenvalue as our value that has been mapped from the complex α plane. The most unstable ω is given as the ω with the largest imaginary part. By applying this procedure, we can determine if given base flows such as the Gaussian wake, have convective or absolute instabilities.

2.3.3 Applications of the Orr-Sommerfeld Equation - Spatial Stability of the Gaussian Wake

An example of determining the spatial stability characteristics of a fluid flow is given by Hultgren and Aggarwal, [12], where they study the nature of absolute instabilities within Gaussian wakes, such as those found behind cylinders in the far field. The velocity distribution for a Gaussian wake profile is given as

$$U(y) = 1 - \lambda e^{-y^2 \ln 2} \tag{2.33}$$

which is valid on the domain $-\infty < y < \infty$. Here, λ is known as the velocity deficit parameter, and varies between 0 and 1. Varying λ equates to changing the distance away from the source of the wake, as can be seen in Figure 2.8.

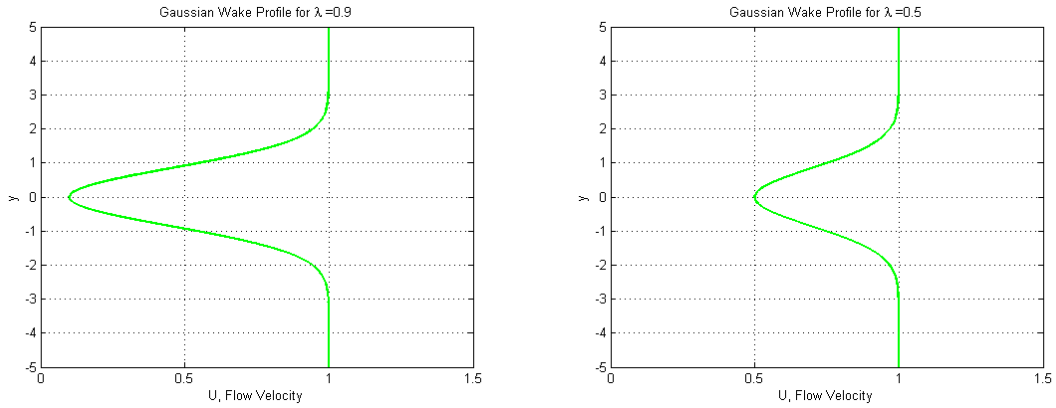

(a) $\lambda = 0.9$ (b) $\lambda = 0.5$

Figure 2.8: Drawing of the Gaussian wake for different values of λ. Here the fluid is moving from left to right.

If we now use this base flow, we can determine the spatial stability characteristics of this flow for different values of the velocity deficit λ. Looking at a value of the Reynolds number of 100, we can now vary λ to see if an absolute instability occurs. In Figure 2.9 we can see how mapping the α plane has formed a cusp in the lower half of the ω plane, showing that no absolute instability exists. However, by increasing the velocity deficit as shown in Figure 2.10, we form a cusp in the upper half of the complex ω plane showing that an absolute instability has formed.

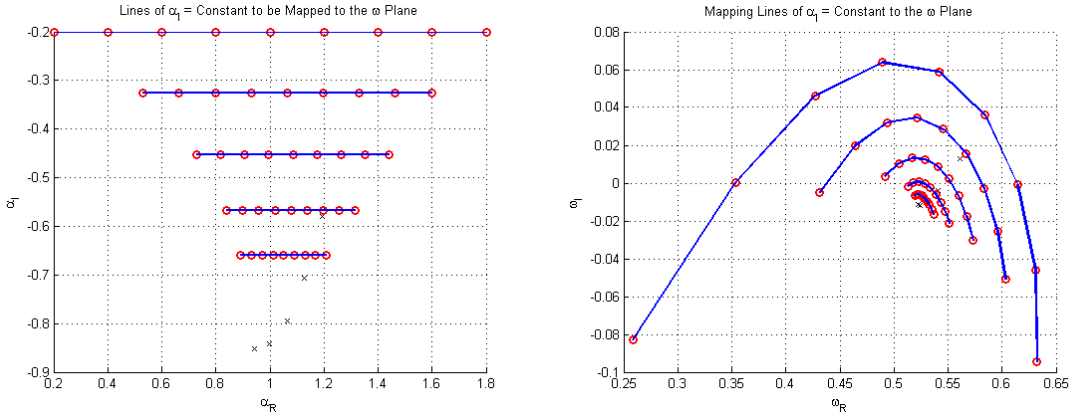

(a) The grid of α values to be mapped (b) α values mapped to the complex ω plane

Figure 2.9: Mapping of the complex α plane to the complex ω plane, for velocity deficit of $\lambda = 0.95$. The 'x' marks where the branch point is in the ω plane, and the pinch point is in the α plane. Notice how the cusp that forms is below the ω_R axis.

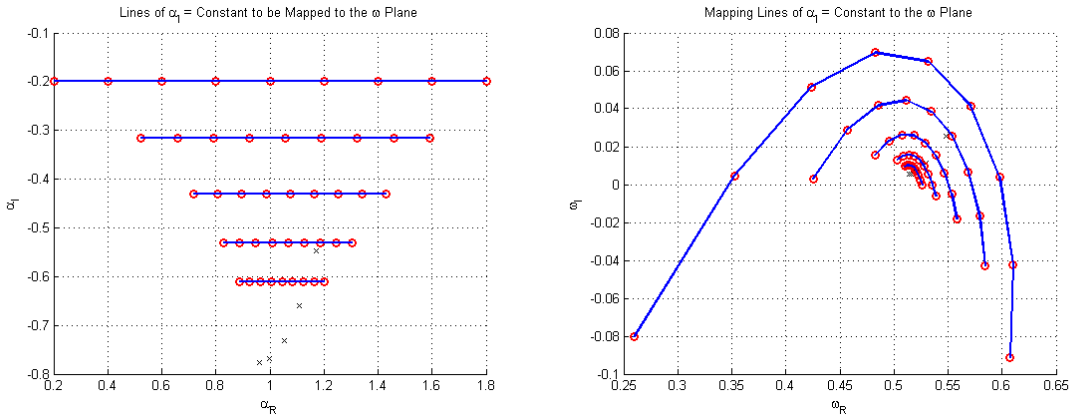

(a) The grid of α values to be mapped (b) α values mapped to the complex ω plane

Figure 2.10: Mapping of the complex α plane to the complex ω plane, for velocity deficit of $\lambda = 0.97$. The 'x' marks where the branch point is in the ω plane, and the pinch point is in the α plane. The cusp in the complex ω plane has now formed above the ω_R axis, hence showing that absolute instabilities now exist.

Chapter 3

Numerical Methods for the Orr-Sommerfeld Equation

As mentioned previously, the Orr-Sommerfeld equation is an ODE eigenvalue problem with properties that can make it very hard to solve in even the simplest cases. It was not until the the 1960's, almost 50 years after the problem was first posed, that accurate solutions to the equation came about. Because the Orr-Sommerfeld equation is a linear ODE, a multitude of methods exist to allow for numerical solutions to the eigenvalues but, as can be expected, certain methods are better suited to solve the proposed problem.

Historically there have been three general approaches to solving the Orr-Sommerfeld equation: shooting methods, finite difference methods, and collocation methods. While all these methods were first applied to solving the temporal stability problem, by using the cusp mapping method, they can be used to also solve the spatial stability problem.

3.1 Finite Difference Methods

The application of finite difference methods to the Orr-Sommerfeld eigenvalue problem is very straight forward and allows for determination of the entire eigenspectra of a problem. The goal is to break the ODE problem into a algebraic eigenvalue problem by taking the derivatives of the normal velocity ϕ to be ap-

proximated by a finite difference schema. First, we rearrange the Orr-Sommerfeld equation as follows

$$\left(-U\alpha^2 - U'' - \frac{\alpha^4}{i\alpha Re}\right)\phi + \left(U + \frac{2alpha^2}{i\alpha \mathrm{Re}}\right)\phi'' - \frac{1}{i\alpha \mathrm{Re}}\phi^{\mathrm{iv}} = c(\phi'' - \alpha^2\phi) \quad (3.1)$$

with the following boundary conditions

$$\phi(\pm 1) = \phi'(\pm 1) = 0 \qquad \text{Channel Flow} \quad (3.2)$$

$$\phi(\pm \infty) = \phi'(\pm \infty) = 0 \qquad \text{Unbounded Flow} \quad (3.3)$$

This allows the eigenvalue problem (2.18) to be written as follows

$$\mathbf{A}\tilde{\phi} = \mathbf{cB}\tilde{\phi} \quad (3.4)$$

where c is now a vector containing all the eigenvalues of the discretized system, $\mathbf{A}$ is a complex matrix, and $\mathbf{B}$ is a real symmetric matrix. In the present research, a second order, central finite difference approximation using constant grid spacing, h, was used making the matrices $\mathbf{A}$ and $\mathbf{B}$ pentagonal, and tridiagonal respectively. Equations (3.5) and (3.6) represent the finite difference approximations of the second and fourth derivatives for use in the Orr-Sommerfeld equation.

$$\phi'(y) = \frac{y_{i-1} - 2y_i + y_{i+1}}{h^2} \quad (3.5)$$

$$\phi^{\mathrm{iv}}(y) = \frac{y_{i-2} - y_{i-1} + 2y_i - y_{i+1} + y_{i+2}}{h^2} \quad (3.6)$$

In order to handle the boundary condition $\phi(\pm 1) = 0$, we simply must remove the first and last rows and columns of both $\mathbf{A}$ and $\mathbf{B}$ (which correspond to $y = \pm 1$). To handle the boundary condition $\phi'(\pm 1)$ is a bit more difficult. Following [4] first we rewrite the derivative boundary condition as follows

$$\phi_0' = \frac{\phi_1 - \phi_{-1}}{2h} \quad (3.7)$$

Now using (3.7) we can write ϕ_{-1} as follows

$$\phi_{-1} = \phi_1 - 2h\phi_0' \quad (3.8)$$

Because from the boundary condition $\phi'(\pm 1) = 0$, we have that $\phi_0' = 0$, so we can write the above equation as

$$\phi_{-1} = \phi_1 \quad (3.9)$$

Solving the general eigenvalue problem (3.4) can be done in a straightforward manner using any number of iterative methods. The advantage of the representation of the Orr-Sommerfeld equation shown in (3.1) is that (3.4) can be left multiplied by $\mathbf{B^{-1}}$ to yield a traditional eigenvalue problem. This can only be done because, as mentioned before, $\mathbf{B}$ is a real symmetric matrix. For the current research, MATLAB's, built in eigenvalue solvers were used to solve the generated algebraic eigenvalue problem.

For benchmarking purposes, the speed and accuracy of the finite difference method used was checked for varying grid sizes against the model problem of the Orr-Sommerfeld equation applied to Plane Poiseuille flow. Figures 3.1, and 3.2 show the speed and accuracy of the finite difference numerical method.

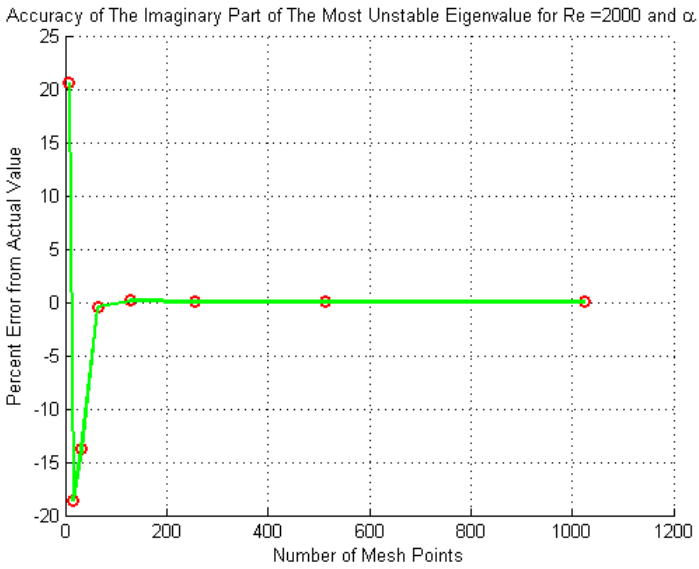

Figure 3.1: Plot showing the accuracy of the finite difference method outlined. The method is solving for the most unstable eigenvalue of plane Poiseuille flow at a Reynolds number 2,000, and $\alpha = 1$. On the x-axis is the grid size, while the y-axis is the percent error from the correct solution given in [18]. Here we see that at 1,024 mesh points, the maximum error obtained in the eigenvalue was only 0.003%.

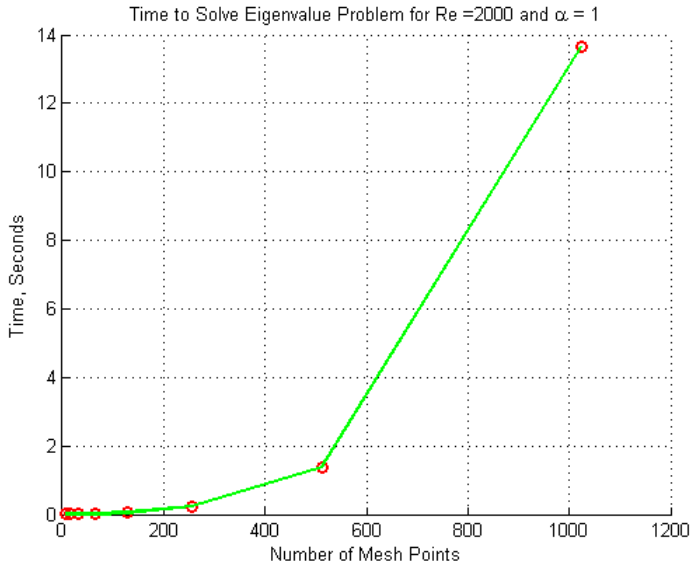

Figure 3.2: Plot showing the speed of the finite difference method outlined. The method is solving for the most unstable eigenvalue of plane Poiseuille flow at a Reynolds number 2,000, and $\alpha = 1$. On the x-axis is the grid size, while the y-axis is the time to solve for the solution.

3.2 Collocation Methods

Collocation methods are a general class of numerical methods that can be applied to many different kinds of ODE's. The general idea of collocation methods is to find a solution to an ODE by approximating the solution as a linear combination of some assumed set of orthogonal functions. This linear combination of orthogonal functions are required to satisfy the ODE at a set of collocation points. Mathematically, this looks like the following

$$\sum_{j=1}^{n} c_j (L v_j)(t_i) = w(t_i) \qquad (1 \leq i \leq n) \tag{3.10}$$

In the above equation, L is a general linear differential operator, v_j is a set of functions, and t_i are the collocation points. There exist a large set of possible choices for v_j, and some common functions that can be picked are the set of polynomials $1, t, t^2, t^3, \ldots$, or B-splines [13]. Specifically with the Orr-Sommerfeld equation, Chebyshev polynomials were found by Orzag [17] to obtain highly accurate results of the eigenvalues for Poiseuille flow, and Couette flow using many less

discretization points then required for finite difference methods. As such, Chebyshev collocation methods have become one of the standard methods for solving for the eigenvalues of the Orr-Sommerfeld equation.

3.2.1 Chebyshev Polynomials

Chebyshev polynomials are a set of orthogonal polynomials defined on the interval ± 1, making them a candidate for use in a collocation method. Chebyshev polynomials of the first kind, $T_k(x)$ are eigenfunctions of the Strum-Liousville [3] problem given as

$$\left(\sqrt{1-y^2}T_k'(y)\right)' + \frac{y^2}{\sqrt{1-y^2}}T_k(y) = 0 \tag{3.11}$$

for any $k \epsilon \mathbb{N}$. Assuming the eigenfunctions are normalized, this gives one representation of the Chebyshve polynomials as

$$T_k(y) = \cos(k\cos^{-1}(y)) \tag{3.12}$$

By expanding the Chebyshev polynomials as a power series, it is possible to rewrite the Chebyshev polynomial in (3.12) as a recursion relation given as

$$T_{k+1}(y) = 2xT_k(y) - T_{k-1}(y) \tag{3.13}$$

$$T_0(y) = 1 \tag{3.14}$$

$$T_1(y) = y \tag{3.15}$$

The derivatives of Chebyshev polynomials can also be given as a recursion relation and look like

$$T_k^{(n)}(y) = 2kT_{k-1}^{(n-1)}(y) + \frac{k}{k-1}T_{k-1}^{n}(y) \qquad n = 3,4,5 \tag{3.16}$$

$$T_0^{(n)}(y) = 0 \tag{3.17}$$

$$T_1^{(n)}(y) = T_0^{(n-1)}(y) \tag{3.18}$$

$$T_2^{(n)}(y) = 4T_1^{(n-1)}(y) \tag{3.19}$$

When Chebyshev polynomials are used for interpolation or collocation methods, they are normally evaluated on a set of points known as Gauss- Lobatto points

which are clustered near the boundary of the domain, ± 1. The Gauss-Lobatto points are given as

$$y_i = \cos\left(\frac{i\pi}{N}\right) \tag{3.20}$$

where N is the number of points being used in the interpolation grid. The use of Gauss-Lobatto points allows for the minimization of Runge's phenomena in interpolation, as well as the advantage of having the boundary layers well resolved for fluid flow problems such as those encountered in channel flow.

Because Chebyshev polynomials are only defined on the interval of ± 1, in order to use them on domains of infinite size, a mapping of the domain ± 1 to a new domain must be used. Normally the maps that are used are either a exponential maps such as

$$y = \tanh^{-} 1(z) \tag{3.21}$$

or algebraic maps such as

$$y = \frac{z}{\sqrt{1 - z^2}} \tag{3.22}$$

It was found by Orzag and Grosch [9] that algebraic maps from $-\infty$ to ∞ tend to be much more accurate then exponential maps, especially for the Orr-Sommerfeld problem. To apply a mapping to solve the Orr-Sommerfeld equation on an infinite domain, it is first necessary to transform the independent variable, y, from the infinite domain to the domain ± 1. For the the hyperbolic tangent map we can write,

$$z = \tanh y, \tag{3.23}$$

where z is in the domain ± 1, while y is in the domain $\pm\infty$. Now applying this mapping to the Orr-Sommerfeld equation, we arrive at the following transformed equation,

$$\frac{1}{\mathrm{Re}}(A\phi + B\phi' + C\phi'' + D\phi''' + E\phi^{\mathrm{iv}}) = i\alpha c('-\alpha^2\phi + F\phi' + G\phi'') \tag{3.24}$$

where A, B, C, D, E , F , and G are given as follows

$$A = \alpha^4 + \alpha^3 i \mathrm{Re} U(y) + i\alpha \mathrm{Re} U''(y) \tag{3.25}$$

$$B = 2\mathrm{sech}^2(y)\tanh(y)\left[2\alpha^2 + \alpha i \mathrm{Re} U + 8\mathrm{sech}^2(y) - 4\tanh^2(y)\right] \tag{3.26}$$

$$C = -\mathrm{sech}^4(y)\left[2\alpha^2 + \alpha i \mathrm{Re} U(y) + 8\mathrm{sech}^2(y) - 28\tanh^2(y)\right] \tag{3.27}$$

$$D = -12\mathrm{sech}^6(y)\tanh(y) \tag{3.28}$$

$$E = \mathrm{sech}^8(y) \tag{3.29}$$

$$F = -2\mathrm{sech}^2(y)\tanh(y) \tag{3.30}$$

$$G = \mathrm{sech}^4(y) \tag{3.31}$$

similarly, the transformed Rayleigh equation can be given more simply as,

$$U(y)\left[-alpha^2\phi - 2\mathrm{sech}^2(y)\tanh(y)\phi' + \mathrm{sech}^4(y)\phi''\right] - U''(y)\phi = \\ -\alpha^2\phi - 2\mathrm{sech}^2\tanh(y)\phi' + \mathrm{sech}^4\phi''$$

Both transformed Orr-Sommerfeld and Rayleigh equations can now be solved as usual for the eigenvalues. In this research, it was found that using this specific map (hyperbolic tangent) for solving the temporal eigenvalue problem would cause significant errors for smaller wave numbers as illustrated in Figure, 3.3. Here we are comparing the eigenvalues obtained by Howard and Drazin [7] for the inviscid Bickley jet flow, given by $U(y) = \mathrm{sech}^2(y)$. To solve this problem using Chebyshev collocation, the transformed Rayleigh equation was used. As we can see, there is a significant amount of error that exists for small α, but for large α the solution is very accurate. One thought as to why such an error exists could be in the fact that small α, which corresponds to larger wavelengths, cannot be accurately represented by this map. Qualitatively, it can be viewed as if the longer wavelength perturbations are being compressed on to the domain ± 1, hence causing significant problems with properly resolving the true eigenvalues associated with these perturbation wavelengths.

In order to alleviate the problem of these eigenvalues associated with smaller wave numbers, the computational grid that is used needs to be very large. Because the hyperbolic tangent or algebraic maps, map the Gauss-Lobatto points to the

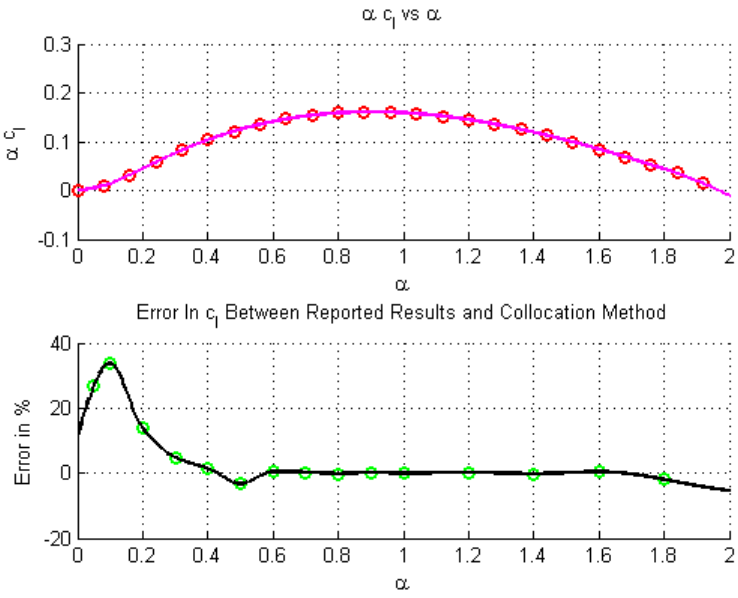

Figure 3.3: Plot showing the error between the expected eigenvalues obtained in [7], and the eigenvalues obtained from solving the transformed Rayleigh equation using Chebyshev collocation.

domain $\pm\infty$, a larger number of Gauss-Lobatto points needs to be used to ensure that enough points at the boundary ± 1 get mapped sufficiently far to infinity. It was found that for accurate computations, the domain size needs to be anywhere from five to fifty times the wake width. Figure 3.4 shows how for the Bickley jet at the critical Reynolds number requires a computational domain that is roughly five times larger then the jet width.

3.2.2 Chebyshev Collocation for the Orr-Sommerfeld Equation

To apply Chebyshev collocation methods to the Orr-Sommerfeld problem given by equations (2.18), we follow [18] and first expand the perturbations ϕ in terms of Chebyshev polynomial as follows,

$$\phi = \sum_{k=0}^{K} a_k T_k(y) \tag{3.32}$$

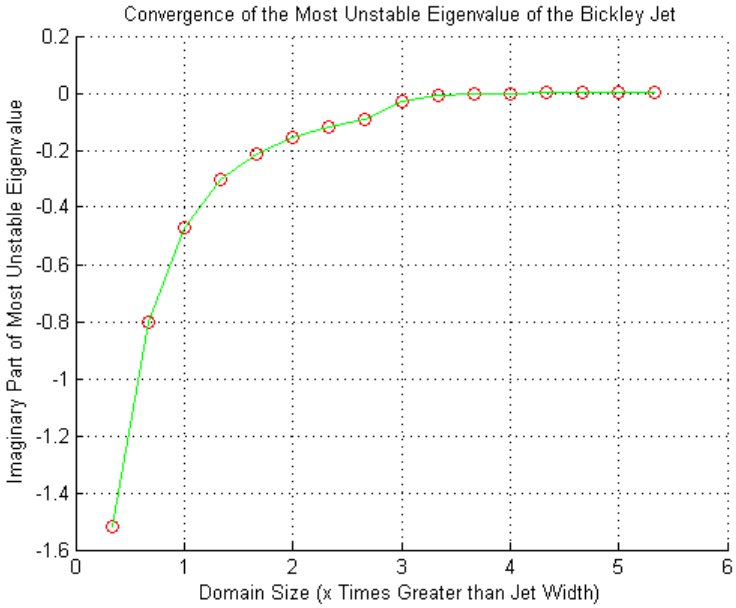

Figure 3.4: Plot showing the imaginary part of the most unstable eigenvalue for the Bickley jet as a function of domain size. The x-axis shows the number of times the domain is larger when compared to the width of the jet.

incorporating into equation (2.18), we arrive at the following Chebyshev discretization of the Orr-Sommerfeld equation,

$$\left(U(y)\alpha^2 - U''(y) - \frac{\alpha^3}{i\mathrm{Re}}\right)\sum_{k=0}^{K} a_k T_k(y) + \left(U(y) + \frac{2\alpha}{i\mathrm{Re}}\right)\sum_{k=0}^{K} a_k T_k''(y) \tag{3.33}$$

$$-\frac{1}{i\alpha\mathrm{Re}}\sum_{k=0}^{K} a_k T_k^{\mathrm{iv}}(y) = c\left(\sum_{k=0}^{K} a_k T_k''(y) - \alpha^2\sum_{k=0}^{K} a_k T_k(y)\right) \tag{3.34}$$

along with boundary conditions given as

$$\sum_{k=0}^{K} a_k T_k(\pm 1) = 0 \tag{3.35}$$

$$\sum_{k=0}^{K} a_k T_k'(\pm 1) = 0 \tag{3.36}$$

To numerically solve equation (3.34) along with the boundary conditions (3.35) and (3.35), we can rewrite the equations as a matrix equation of the form

$$\mathbf{A}\tilde{\phi} = \mathbf{B}\tilde{\phi} \tag{3.37}$$

Here $\mathbf{A}$ has the following form

$\mathbf{A} =$

$$\begin{pmatrix} T_0(1) & T_1(1) & \dots \\ T_0'(1) & T_1'(1) & \dots \\ A_{y_2}T_0(y_2) + B_{y_2}T_0''(y_2) - C_{y_2}T_0^{\text{iv}}(y_2) & A_{y_2}T_1(y_2) + B_{y_2}T_1''(y_2) - C_{y_2}T_1^{\text{iv}}(y_2) & \dots \\ \vdots & \vdots & \dots \\ T_0(-1) & T_1(-1) & \dots \\ T_0'(-1) & T_1'(-1) & \dots \end{pmatrix}$$

where A_y, B_y and C_y are as follows,

$$A_y = U(y)\alpha^2 - U''(y) - \frac{\alpha^3}{i\text{Re}} \tag{3.38}$$

$$B_y = U(y) + \frac{2\alpha}{i\text{Re}} \tag{3.39}$$

$$C_y = \frac{1}{i\alpha\text{Re}} \tag{3.40}$$

$\mathbf{B}$ has the following form

$$\mathbf{B} = \begin{pmatrix} T_0(1) & T_1(1) & \dots \\ T_0'(1) & T_1'(1) & \dots \\ T_0''(y_2) - \alpha^2 T_0(y_2) & T_1''(y_2) - \alpha^2 T_1(y_2) & \dots \\ \vdots & \vdots & \dots \\ T_0''(y_{n-2}) - \alpha^2 T_0(y_{n-2}) & T_1''(y_{n-2}) - \alpha^2 T_1(y_{n-2}) & \dots \\ T_0(-1) & T_1(-1) & \dots \\ T_0'(-1) & T_1'(-1) & \dots \end{pmatrix}$$

An easier method of writing both $\mathbf{A}$ and $\mathbf{B}$ is as follows,

$$\mathbf{A} = A_y\mathbf{D}^0 + B_y\mathbf{D}^2 - C_y\mathbf{D}^4 \tag{3.41}$$

$$\mathbf{B} = \mathbf{D}^0 + \alpha^2\mathbf{D}^2 \tag{3.42}$$

Here, $\mathbf{D}^N$ is known as a differentiation matrix, and is simply a full matrix that has the derivatives of the Chebeyshev polynomials evaluated at the Gauss-Lobatto collocation points.

One of the primary advantages of writing the matrix problem using differentiation matrices is that a recursion algorithm can be used to obtain the N^{th} derivative matrix efficiently. However, the primary drawback of using the differentiation matrices, and collocation methods in general, is that they generate full matrices, which for larger N, can be extremely ill-conditioned causing significant problems with roundoff error.

Figures 3.6 and 3.5 show the speed and accuracy of a Chebyshev collocation based solver for the Orr-Sommerfeld equation. As can be seen, with only 128 mesh points, 8 times less the number of mesh points as compared the finite difference method, the Chebyshev collocation method was able to obtain an error of only $3.7 \times 10^{-5}\%$. Also the total time taken to obtain this result, was far less then a tenth of a second, compared to close to 13 seconds for the finite difference method.

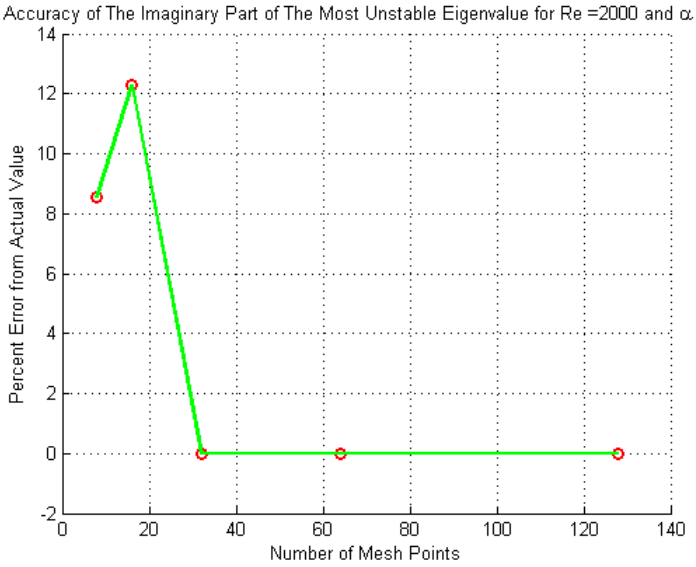

Figure 3.5: Plot showing the accuracy of the Chebyshev collocation method outlined. The method is solving for the most unstable eigenvalue of plane Poiseuille flow at a Reynolds number 2,000, and $\alpha = 1$. On the x-axis is the grid size, while the y-axis is the percent error from the correct solution given in [18]. Here we see that at 128 mesh points, the maximum error obtained in the eigenvalue was $3.7 \times 10^{-5}\%$.

Because of the speed and efficiency of the Chebyshev based solver, it was

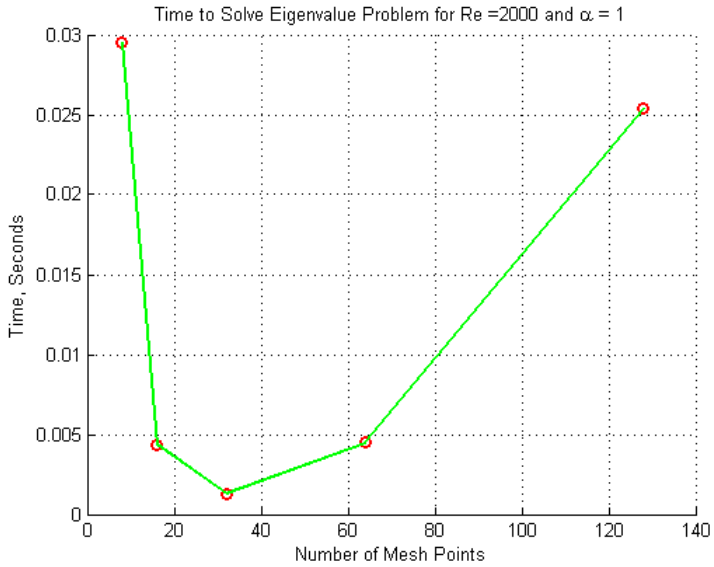

Figure 3.6: Plot showing the speed of the Chebyshev collocation method outlined. The method is solving for the most unstable eigenvalue of plane Poiseuille flow at a Reynolds number 2,000, and $\alpha = 1$. On the x-axis is the grid size, while the y-axis is the time to solve for the solution.

decided that for this research, Chebyshev collocation methods should be used. However, as will be seen later, the flow profile that was being studied had a very complex structure, and as such was very difficult to solve. To help make solving the stability characteristics of this specific wake profile simpler, it was decided to use an available solver known as Chebfun, for MATLAB. While Chebfun still solves ODE's using collocation methods, it has been optimized to handle very general and large problems efficiently and in an easy to use manner.

3.2.3 Chebfun

Chebfun is an open source software suite developed by the numerical analysis group at Oxford University which overloads a broad set of MATLAB functions for use using structures known as chebfuns. Chebfun's are essentially Chebyshev discretization of functions, and by passing overloaded MATLAB functions chebfun structures, the functions can operate on these structures much like they would operate on normal numbers. The advantage with the Chebfun package for use

with the Orr-Sommerfeld equation is its ability to solve ODE eigenvalue problems quickly and efficiently on almost any size domain. Chebfun has the ability to handle a variety of boundary conditions, as well as the ability to use a form of adaptive meshing which is also very beneficial to computing accurate solutions to the Orr-Sommerfeld equation.

Creating a chebfun structure is very straightforward, and only involves specifying the function that is being operated on, and the domain on which the function exists in. Below is an example of creating a chebfun for the equation $y = \sin(2x)/2x$

```
1 dom = [-10 10] %Define the domain on which the equation is valid
2 f = chebfun(@(x) 'sin(2*x)/(2*x)',dom); %Define the chebfun
3 figure; %Plot the function
4 hold on; grid on;
5 plot(f,'g'); plot(f,'*r')
```

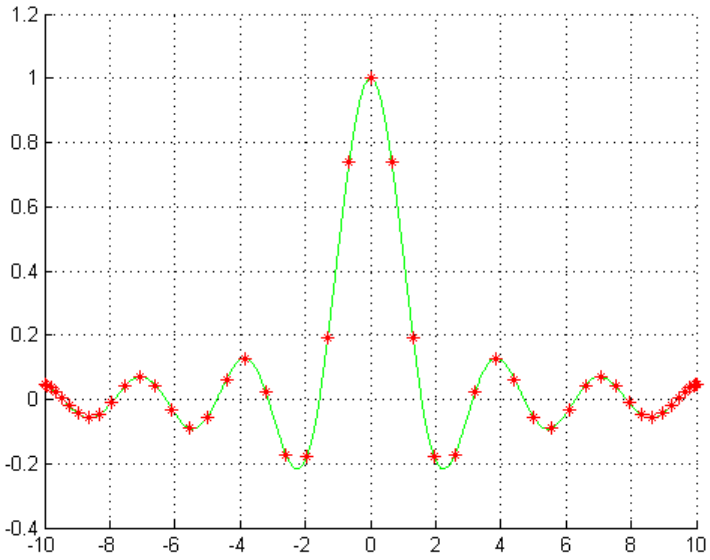

Figure 3.7: Plot of $\sin(2x)/(2x)$ using chebfuns. The red asterisk show where chebfun has picked the collocation points to located. Notice the bunching of points near the end points due to the use of Gauss-Lobatto points to minimize Runge error.

Now that the chebfun has been created, any number of manipulation of the function can be done, such as differentiation and integration. For example, in order to take the second derivative of $y = \sin(2x)/2x$ the command `diff` can be used as follows,

```
1 fpp = diff(f,2); %Take the second derivative of f
2 figure; %Plot f and it's second derivative
3 hold on; grid on;
4 plot(f,'g'); plot(fpp,'c');
5 plot(f,'*r'); plot(fpp,'*k');
```

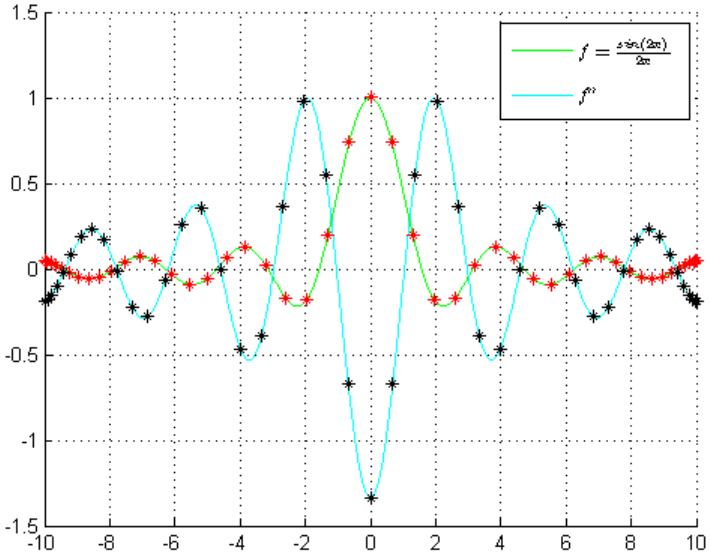

Figure 3.8: Plot of $\sin(2x)/(2x)$ and its second derivative using chebfuns. The red and black asterisks show where chebfun has picked the collocation points. Again, notice how the points are clustered near the endpoints to prevent Runge error.

The overloaded `diff` function handles derivatives in a very efficient manner by making use of FFT's to solve for the derivatives of the function.

One of the chebfun packages' advantage is the speed at which it can solve ODE's on a domain of varying size. For the temporal Orr-Sommerfeld equation, we can easily solve for the eigenvalues of plane Poiseuille flow by doing the following,

```
dom = [-1 1];                    %Define the Domain
uX = chebfun(@(x) 1-x.^2,dom);   %Define the flow Profile, U
uXpp = diff(uX,2);               %Define second derivative of U
Re = 7000;                       %Define the Reynolds number
alpha = 1.02;                    %Define the wave number
A = chebop(dom);                 %Define the a chebop structure's
                                 %domain
A.op = @(x,u) ...                %Define the LHS of the OS equation
    (diff(u,4) - 2*alpha^2*diff(u,2) ...
    + alpha^4*u)/Re ...
    - 1i*alpha*((uX(x)).*(diff(u,2) - alpha^2*u) - (uXpp(x)).*u);
B = chebop(dom);                 %Define the a chebop structure's
                                 %domain
B.op = @(x,u) ...                %Define the LHS of the OS equation
    diff(u,2) - alpha^2*u;
A.lbc = @(u) [u , diff(u)];      %Implement the boundary conditions
                      %A
A.rbc = @(u) [u , diff(u)];
[V e] = eigs(A,B,100,'LR');      %Solve the the most unstable
                                 %eigenvalues
e = diag(e);
[maxe l]= max(real(e));
e = e/(-1i*alpha);
```

In this code we define a structure known as a chebop which is used to define a linear operator that is the differentiation equation we are trying to solve. In this case we have two chebops. A, which defines the left-hand side of the Orr-Sommerfeld equation, and B, which define the right-hand side of the Orr-Sommerfeld equation. The chebop structure contains all the information about the linear operator we are trying to solve, such as the domain on which the operator lives on, and the boundary conditions. To solve the eigenvalue problem all we need to do is pass the chebop structure to the `eigs` function in MATLAB which has been overloaded to handle a chebop structure.

For this research, the flow profile which we are interested in has a domain of $(-\infty, +\infty)$, and as it turns out, solving this problem accurately requires a very fine

computational grid, especially near the wake which is located at the origin. To help reduce the size of the grid, we took advantage of the fact that the solutions we are looking for come in both odd and even modes, so we can solve the Orr-Sommerfeld equation on the domain $[0, +\infty]$, allowing us to cut the computational grid in half. The issue now is we need to solve for two types of modes, the even mode, which is symmetric about the origin, and the odd mode, which is anti-symmetric about the origin. To do this we supply two different boundary conditions at 0. For the symmetric mode, the boundary condition at 0 is as follows:

$$\phi'(0) = 0 \qquad \phi'''(0) = 0, \tag{3.43}$$

while the boundary conditions for the anti symmetric mode at 0 are as follows,

$$\phi(0) = 0 \qquad \phi''(0) = 0. \tag{3.44}$$

Implementing these boundary conditions is very straight forward using the Chebfun package. As can be seen in the previous code, all that is necessary is to specify the left and right boundary conditions as a function of u in the chebop structure. So for example to implement the boundary conditions in (3.43), we do the following,

```
1 A.lbc = @(u) [diff(u) , diff(u,3)];  %Boundary Condition at 0
2 A.rbc = @(u) [u , diff(u)];  %Boundary Condition at Infinity
```

Chapter 4

Stability of Self-Propelled Wakes

Self-Propelled wakes are found in many different physical systems, such as the wakes behind fish or submarines, and have the important characteristic of being momentum-less.

4.1 Wakes Behind Fish

The wake behind a fish normally will consists of a very non-linear and complex flow, however if we look at the far field behind the fish, then we can approximate the wake to be a parallel shear flow generated by a force doublet. Following the work done by Afanasyev [1], Smirnov and Voropayev [19], the derivation of the flow behind a force doublet can be determined by first starting with two single forces delivering some amount of kinematic momentum, I, to the fluid. A single force with finite kinematic momentum in the x-direction, centered at the origin in two dimensions will have the following associated stream function,

$$\psi = \frac{Iy}{2\pi(x^2+y^2)}\left(1-e^{-\xi^2}\right). \tag{4.1}$$

Here ξ is given as

$$\xi = \sqrt{\frac{x^2+y^2}{4\nu t}}. \tag{4.2}$$

In a force doublet, there are two single forces acting in opposite directions of each other, and infinitesimally close to each other. Thus, to obtain the stream function

for a force doublet, we take the limit as two single forces approach each other along the x-direction as follows,

$$\psi_{\text{Force Doublet}} = \psi(x, y, t) - \psi(x + \epsilon, y, t). \tag{4.3}$$

As $\epsilon \to 0$, this yields the stream function for a force doublet as

$$\psi = -\frac{Mxy}{\pi(x^2 + y^2)^2}\left[1 - (1 + \xi^2)e^{-\xi^2}\right]. \tag{4.4}$$

In the above equations we have that x and y are the stream-wise and span-wise coordinates, t is time, ν is the kinematic viscosity, and M is the instantaneous intensity of the force doublet. Because we wish to obtain the wake profile of a force doublet moving at velocity U, we will have to integrate equation (4.4) through time. Upon doing this integration, M will be transformed such that it will represent the force doublet acting continuously through time. We will refer to this new variable as Q, which has units of $[Q] = L^4/t^2$. Below is a table of all the constants and variables for the above equations, along with their corresponding units.

Constant	Units
M	$\left[\frac{L^4}{T}\right]$
ν	$\left[\frac{L^2}{T}\right]$
U	$\left[\frac{L}{T}\right]$

Variable	Units
y	$[L]$
x	$[L]$
t	$[T]$
ψ	$\left[\frac{L^2}{T}\right]$

Before continuing, it is important that we first non-dimensionalize (4.4) for use in the Orr-Sommerfeld equation, so we introduce a length scale, L_0, given as follows,

$$L_0 = \frac{Q^{2/3}}{U\nu^{1/3}}. \tag{4.5}$$

This length scale is related to the length of the fish, and not necessarily the wake width, which is traditionally used to determine the wake Reynolds number. The

choice of this length scale is because the force doublet intensity, which is essentially related directly to the swimming fish, shows up explicitly in the equation of the momentum-less wake profile. Thus, it makes sense to relate the fish size, to the wake profile as well. Using this length scale, we can now define our non-dimensional variables as follows:

$$\bar{x} = \frac{x}{L_0}, \quad \bar{y} = \frac{y}{L_0} \quad \text{and} \quad \bar{t} = \frac{U}{L_0}t \tag{4.6}$$

Thus we can write that $y = \bar{y}L_0$, $x = \bar{x}L_0$ and $t = \frac{L_0}{U}\bar{t}$. Starting with ξ we can start to non-dimensionalize each term of equation. Substituting for our non-dimensional variables into ξ, we get the following:

$$\bar{\xi} = \sqrt{\frac{(L_0\bar{x})^2 + (L_0\bar{y})^2}{4\nu(L_0/U)\bar{t}}} \tag{4.7}$$

$$= \frac{1}{2}\sqrt{\frac{L_0U}{\nu}}\sqrt{\frac{\bar{x}^2 + \bar{y}^2}{\bar{t}}}. \tag{4.8}$$

Now we can define our first non-dimensional term, the Reynolds number,

$$\mathrm{Re} = \frac{L_0U}{\nu}, \tag{4.9}$$

So we can now rewrite $\bar{\xi}$ as

$$\bar{\xi} = \frac{1}{2}\sqrt{\mathrm{Re}}\sqrt{\frac{\bar{x}^2 + \bar{y}^2}{\bar{t}}}. \tag{4.10}$$

If we now replace, ξ, x, y with $\bar{\xi}$, $\bar{x}$, and $\bar{y}$ respectively, in equation (4.4), we obtain the following,

$$\psi = -\frac{M(\bar{x}L_0)(\bar{y}L_0)}{\pi((\bar{x}L_0)^2 + (\bar{y}L_0)^2)^2}\left[1 - \left(1 + \left(\frac{1}{2}\mathrm{Re}\sqrt{\frac{\bar{x}^2 + \bar{y}^2}{\bar{t}}}\right)^2\right)e^{-\left(\frac{1}{2}\mathrm{Re}\sqrt{\frac{\bar{x}^2+\bar{y}^2}{\bar{t}}}\right)^2}\right] \tag{4.11}$$

$$= -\frac{M\bar{x}\bar{y}}{\pi L_0^2(\bar{x}^2 + \bar{y}^2)^2}\left[1 - \left(1 + \left(\frac{1}{2}\mathrm{Re}\sqrt{\frac{\bar{x}^2 + \bar{y}^2}{\bar{t}}}\right)^2\right)e^{-\left(\frac{1}{2}\mathrm{Re}\sqrt{\frac{\bar{x}^2+\bar{y}^2}{\bar{t}}}\right)^2}\right]. \tag{4.12}$$

Because the stream function, ψ, has units of $[L^2/T]$, we define $\bar{\psi}$ as follows,

$$\bar{\psi} = \frac{1}{UL_0}\psi \tag{4.13}$$

Rearranging the above equation, we get $\psi = UL_0\bar{\psi}$. Replacing ψ with $UL_0\bar{\psi}$ into equation (4.12) and dividing by UL_0, we get the following

$$\bar{\psi} = -\frac{M\bar{x}\bar{y}}{\pi UL_0^3(\bar{x}^2+\bar{y}^2)^2}\left[1-\left(1+\left(\frac{1}{2}\mathrm{Re}\sqrt{\frac{\bar{x}^2+\bar{y}^2}{\bar{t}}}\right)^2\right)e^{-\left(\frac{1}{2}\mathrm{Re}\sqrt{\frac{\bar{x}^2+\bar{y}^2}{\bar{t}}}\right)^2}\right] \tag{4.14}$$

Now, to obtain the stream-wise velocity profile, we need to find $\partial\psi/\partial y$ which is now equivalent to finding $\partial\bar{\psi}/\partial\bar{y}$. Calculating $\partial\bar{\psi}/\partial\bar{y}$, and substituting in equation (4.8) into equation (4.14), and simplifying, we get

$$\frac{\partial\bar{\psi}}{\partial\bar{y}} = \frac{M\bar{x}}{\pi UL_0^3(\bar{x}^2+\bar{y}^2)^3}e^{-\bar{\xi}^2}\left[\left(e^{-\bar{\xi}^2}-1\right)\left(\bar{x}-3\bar{y}^2\right)-\bar{\xi}^2\left(\bar{x}-3\bar{y}^2\right)+\frac{\bar{y}^2}{2}\bar{\xi}^4\right]. \tag{4.15}$$

Now to get the velocity profile from a continuous force doublet moving with unit velocity in the x direction, we integrate equation (4.15) as shown in Afanasyev [1]

$$\bar{u_x}(\bar{x},\bar{y},\bar{t}) = \int_0^{\bar{t}}\frac{\partial\bar{\psi}}{\partial\bar{y}}\left[\bar{x}-(\bar{t}-\tau),y,(\bar{t}-\tau)\right]\mathrm{d}\tau. \tag{4.16}$$

Because we are integrating with respect to time, we need to multiply equation (4.16) by our time scale $T = L_0/U$. Multiplying equation (4.16) by L_0/U and pulling out all of the constants yields the following

$$\bar{u_x}(\bar{x},\bar{y},\bar{t}) = \frac{Q}{\pi U^2L_0^2}\int_0^{\bar{t}}\frac{\partial\bar{\psi}}{\partial\bar{y}}\left[\bar{x}-(\bar{t}-\tau),y,(\bar{t}-\tau)\right]\mathrm{d}\tau. \tag{4.17}$$

Here M has become Q, the force doublet intensity acting continuously in time, because of the integration. For this integration, it is also important to note that we wish to integrate to $t = \infty$ as that will result in a force doublet moving in time, and ignoring all transient behavior of the flow, i.e. the flow start up. Numerically, the integration was taken to a time that was found sufficiently large enough to generate a steady state flow ($t = 500$).

Now we know that we can write the force doublet intensity as follows:

$$Q = U^2L^2\frac{1}{\sqrt{\mathrm{Re}}}, \tag{4.18}$$

using this relation we can rewrite the term in front of the integral such that we arrive at the following equation,

$$\bar{u_x}(\bar{x},\bar{y},\bar{t}) = \frac{1}{\pi \mathrm{Re}} \int_0^{\bar{t}} \frac{\partial \bar{\psi}}{\partial \bar{y}} \left[\bar{x} - (\bar{t}-\tau), y, (\bar{t}-\tau)\right] \mathrm{d}\tau \tag{4.19}$$

Thus, the final equation for the stream-wise velocity of the wake is given as

$$\begin{aligned} \bar{u_x} =& 1 + \frac{1}{\pi \mathrm{Re}} \int_0^{\bar{t}} \frac{\bar{x}}{(\bar{x}^2+\bar{y}^2)^3} e^{-\bar{\xi}^2} \\ & \left[\left(e^{-\bar{\xi}^2}-1\right)\left(\bar{x}-3\bar{y}^2\right) - \bar{\xi}^2\left(\bar{x}-3\bar{y}^2\right) + \frac{\bar{y}^2}{2}\bar{\xi}^4\right] \left[\bar{x} - (\bar{t}-\tau), y, (\bar{t}-\tau)\right] \mathrm{d}\tau, \end{aligned} \tag{4.20}$$

with ξ, Re, and L_0 given as,

$$\bar{\xi} = \frac{1}{2}\sqrt{\mathrm{Re}}\sqrt{\frac{\bar{x}^2+\bar{y}^2}{\bar{t}}} \qquad \mathrm{Re} = \sqrt{\frac{L_0 U}{\nu}} \qquad L_0 = \frac{Q^{2/3}}{U\nu^{1/3}} \tag{4.21}$$

Note that a one has been added to $\bar{u_x}$ in equation (4.20) to account for the fish frame of reference. Our final equation is now a function of two parameters, the Reynolds number, Re, and $\bar{x}$. y is simply the span-wise coordinate, and equation (4.20) is solved at every y station to determine the stream-wise velocity profile. Varying the two parameters, Re, and $\bar{x}$, we can control the shape of the velocity profile of the wake as can be seen in Figures 4.1 and 4.2. In Figure 4.1 we can see how varying the Reynolds number changes the wake width but the wake velocity is not greatly affected. However, in figure 4.2 we can see how varying $\bar{x}$ drastically effects the maximum and minimum values of the wake velocity, and appears to have a smaller effect then Reynolds number on the wake width.

The reduction in wake width as the Reynolds number is increased makes intuitive sense from the point of view that, as the Reynolds number is increased, by equation (4.18) the force doublet intensity created by the fish is less. Thus, the fish requires less effort to move through the water and is a more efficient swimmer. This reduced amount of effort can be seen through the smaller disturbance of the fluid flow (smaller wake width) and hence less energy used. The reduction in peak velocity as caused by an increase in $\bar{x}$ also makes intuitive sense because, as one would expect, the velocity will be damped as you move further away from the originating source of the fluid flow.

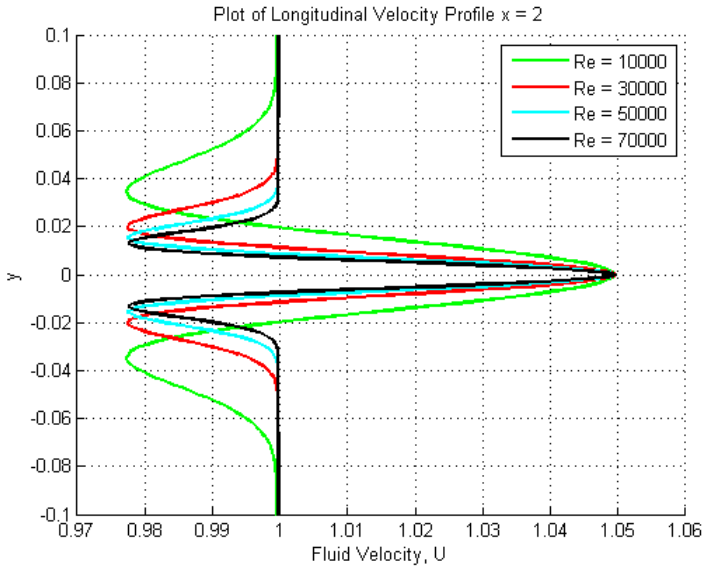

Figure 4.1: $\bar{x}$ is constant ($\bar{x} = 2$) , while the Reynolds number, Re is varied between 10,000 and 70,000

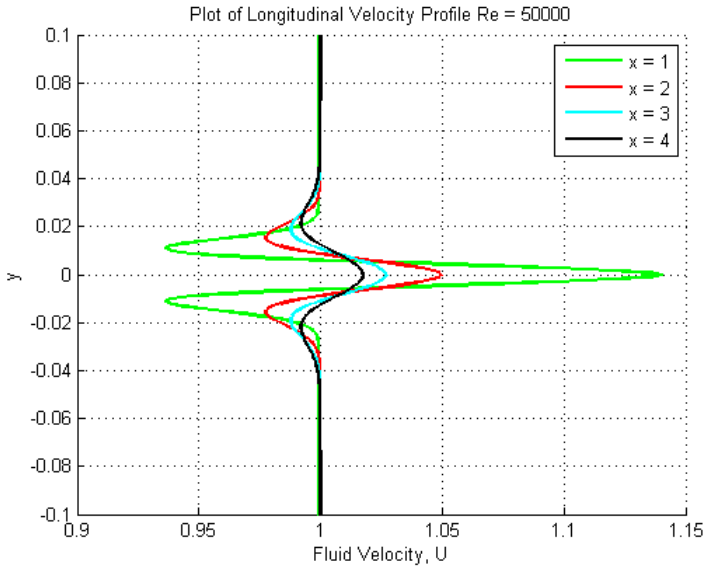

Figure 4.2: The Reynolds number is kept constant (Re$= 50,000$), while $\bar{x}$ is varied between 1 and 4.

4.2 Temporal Stability

Studying the stability of the wake profile, (4.20) was accomplished by using the Chebfun MATLAB package to solve the Orr-Sommerfeld equation. The prob-

lem was challenging to solve due to the difficulty of integrating equation (4.20) as well as the fact that the flow profile shape is coupled to the Reynolds number. As the Reynolds number was changed, the wake width would change, forcing the computational domain size to be increased to allow for the accurate determination of the eigenvalues to the Orr-Sommerfeld equation. Despite this fact, the marginal stability curve was determined for the momentum-less wake profile at various $\bar{x}$ locations as shown in Figures 4.3 and 4.4. In both figures it is interesting to note the two islands of instabilities, the first island forming at lower α values, while the second island of instability forming a much higher α values.

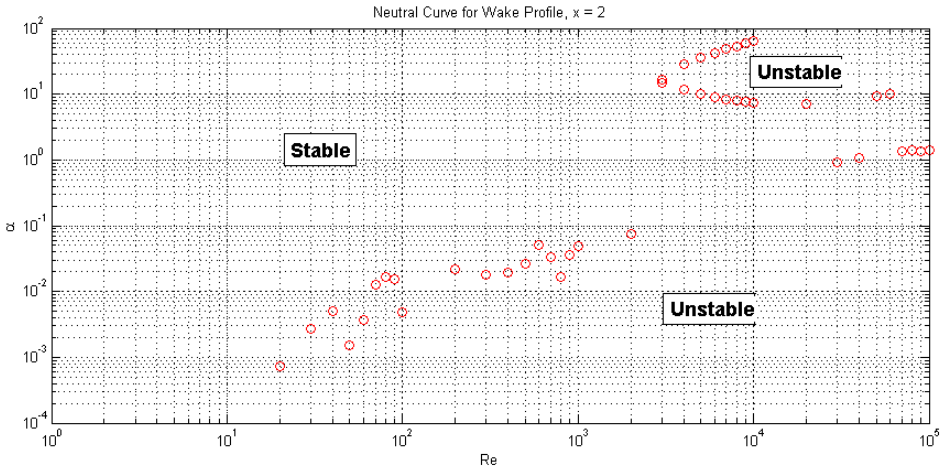

Figure 4.3: The marginal stability curve of the non-dimensional momentum-less wake profile given by equation (4.20). Here $\bar{x} = 2$.

One possible explanation of this second island of instability forming at much higher α values and Reynolds numbers, is that the wake width is much smaller at higher Reynolds numbers. Because of this smaller wake width, smaller wavelengths (larger α) can have more of a destabilizing effect on the wake because the wavelengths are on the same order of magnitude in size as the wake. If for example we look at the wake profile at a Reynolds number of $\mathrm{Re} = 50,000$, we can see that roughly speaking the wake width is on the order of 0.1 units. Now, if there is a perturbation with a wave number of $\alpha = 16$, we would have that this perturbation has a wavelength of roughly 0.06 units, or 60% of the wakes width. Naively then, we would expect that some sort of instability will form because the

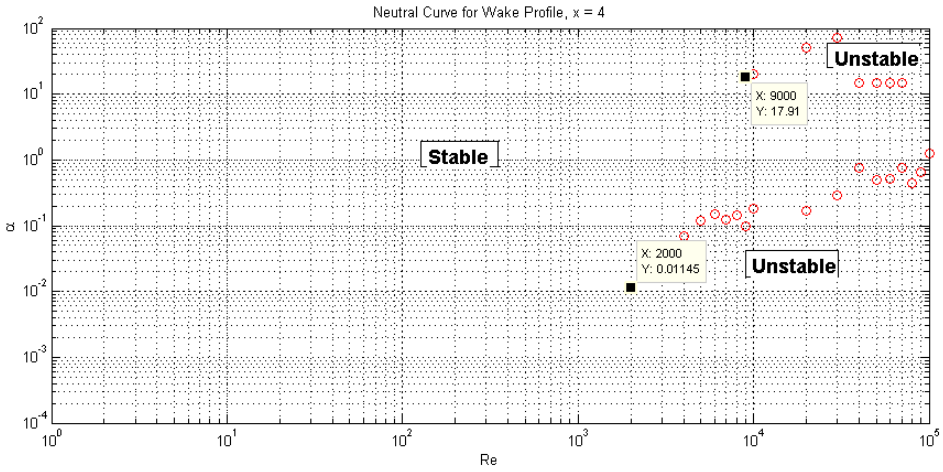

Figure 4.4: The marginal stability curve of the non-dimensional momentum-less wake profile given by equation (4.20). Here $\bar{x} = 4$.

perturbation has a size on the same order as the wake.

It is also interesting to look at the mode shapes, and eigenvalue spectrum for various pairs of α and Re. Figures 4.5 through 4.10 show both the eigenvalue spectrum and mode shapes for the most unstable eigenvalue, for various α and Re values. If we look closely at the eigenvalue spectrum in Figures 4.5, 4.7, and 4.9 we can see both the continuous and discrete spectrum of the eigenvalues. The "blurriness" of the continuous spectrum is most likely caused by a smaller computational domain in relation to the wave number. For example, looking at Figure 4.7, or 4.9, we see that the continuous spectrum is fairly well resolved with wave numbers, α larger then 1, however, in the case of Figure 4.5, where the wave number is $\alpha = 0.6$, we can see that the continuous spectrum is not as well established.

4.3 Spatial Stability

While the temporal stability characteristics of the wake flow studied were interesting, the spatial stability characteristics did not show any such points of interest. In particular, using the cusp map method, no singularities were found in the upper half of the complex ω plane, suggesting that there does not exist any absolute instabilities in the wake flow. This would seem fairly counter intuitive,

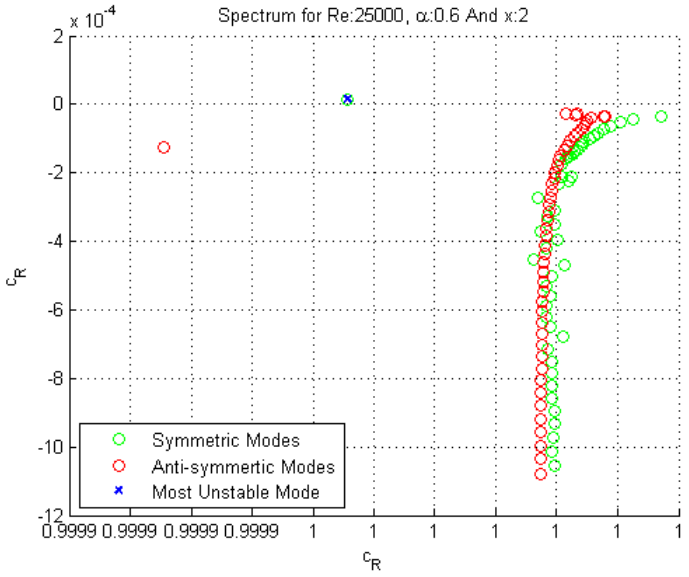

Figure 4.5: Eigenvalue spectrum for $\bar{x} = 2$, $\mathrm{Re} = 25,000$, and $\alpha = 0.6$. These values correspond to an unstable flow.

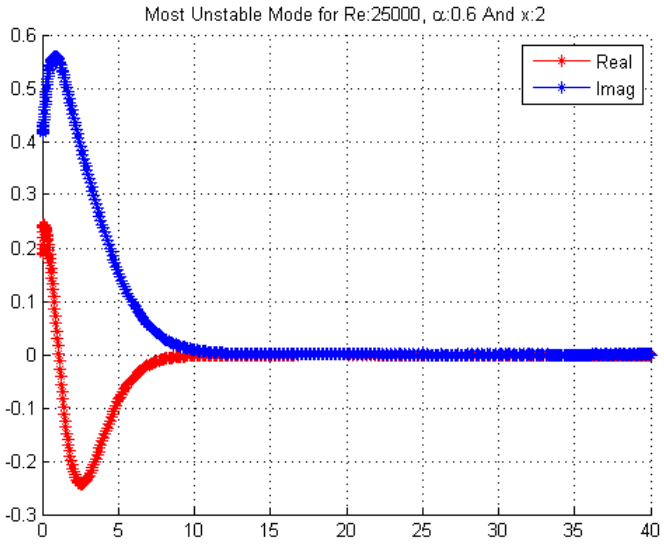

Figure 4.6: Mode shapes for the most unstable eigenvalue shown in Figure 4.5. Here we have $\bar{x} = 2$, $\mathrm{Re} = 25,000$, and $\alpha = 0.6$.

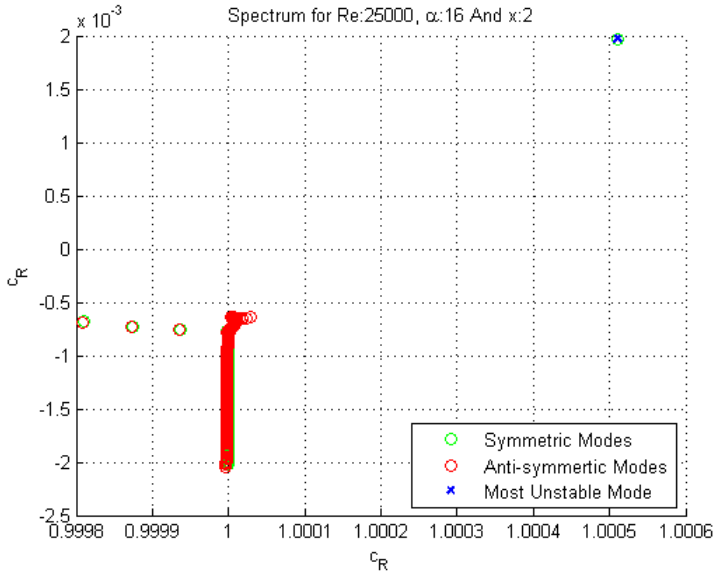

Figure 4.7: Eigenvalue spectrum for $\bar{x} = 2$, $\mathrm{Re} = 25,000$, and $\alpha = 16$. These values correspond to an unstable flow.

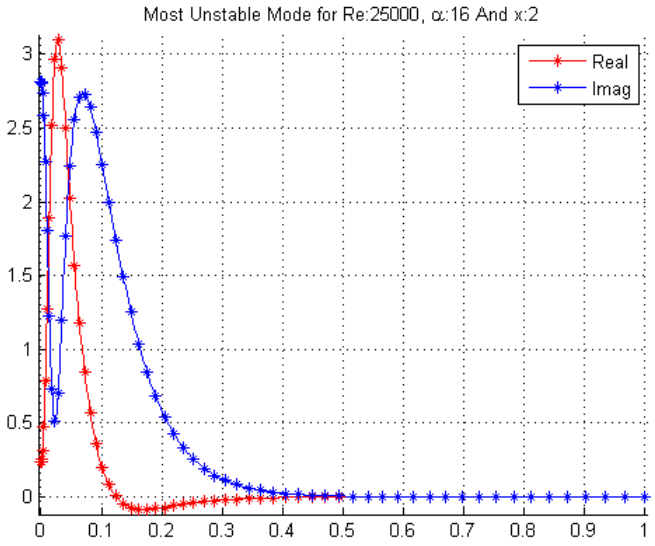

Figure 4.8: Mode shapes for the most unstable eigenvalue shown in Figure 4.5. Here we have $\bar{x} = 2$, $\mathrm{Re} = 25,000$, and $\alpha = 16$.

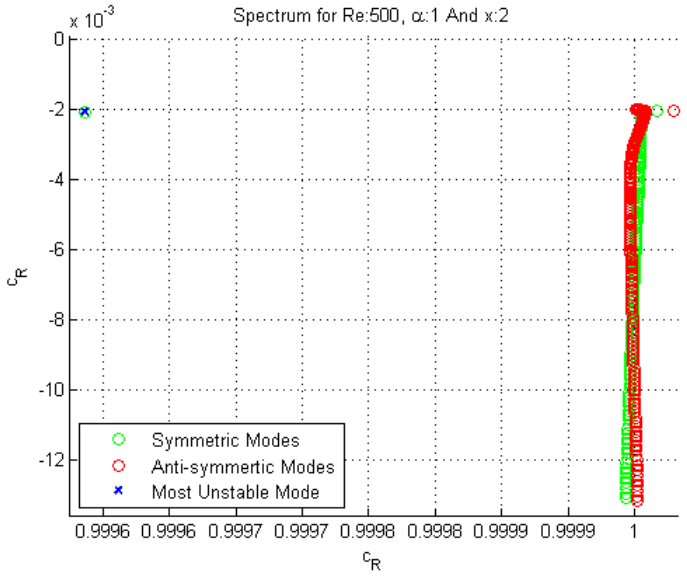

Figure 4.9: Eigenvalue spectrum for $\bar{x} = 2$, Re $= 500$, and $\alpha = 1$. These values correspond to a stable flow.

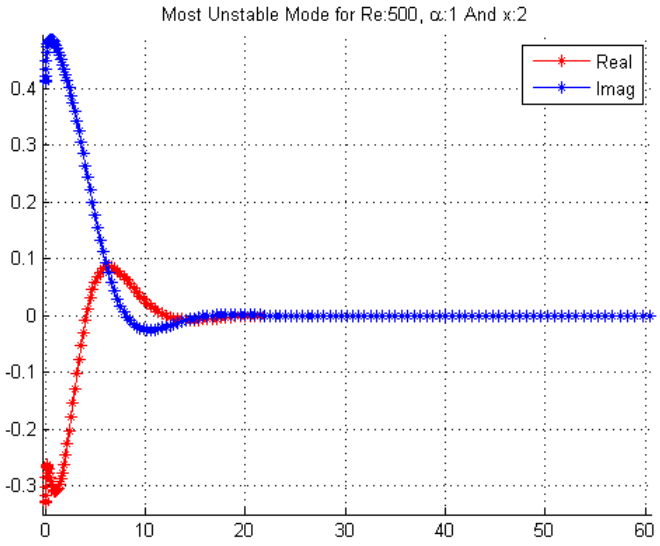

Figure 4.10: Mode shapes for the most unstable eigenvalue shown in Figure 4.5. Here we have $\bar{x} = 2$, Re $= 500$, and $\alpha = 1$.

given the fact that many other wake flows show such absolute instabilities.

Following Criminale, [5], the polynomial eigenvalue problem was also attempted, rather than looking only for singularities in the complex ω plane. However, solving the polynomial eigenvalue problem via matrix methods i.e. Chebyshev and Finite Difference Methods, for the momentum-less wake profile proved to be very challenging and did not reveal meaningful results. A more appropriate method to solve this polynomial eigenvalue problem may be the local method known as the compound matrix method.

Chapter 5

Conclusion

In this research a preliminary study was undertaken to try and better understand the stability characteristics of wakes behind self-propelled bodies, also know as momentum-less wakes. The equation used to model the span-wise velocity profile of the wake yielded very interesting marginal stability curves in the temporal study of the wake stability, yet seems to have no spatial instabilities present. Through the course of this work, two common methods of solving the Orr-Sommerfeld equation were studied to try and determine which method would be the most efficient for flows in the unbounded domain. While both finite difference methods and Chebshev collocation methods have their pros and cons, it was determined that the availability of code for using Chebyshev collocation, and its relative ease of use made it more desirable for this research.

5.1 Future Work

The method of studying hydrodynamic stability used in this research, namely the use of the Orr-Sommerfeld equation, has been around now for over 100 years. While studying the stability characteristics of self propelled wakes is very useful for a wide range of topics, more modern methods of determining the wake stability characteristics exist. More recently with the advent of more powerful computers, the use of DNS simulations allow for even more accurate modeling of the wake behind a self-propelled body, and the wake's response to perturbations.

The analysis done in this thesis was all assuming two dimensional parallel flow, while in actuality, the flow behind self-propelled objects is realistically much more 3 dimensional and non-parallel. As such, much more detailed wake models are needed, and much more robust machinery is required to do the analysis. In this case a full DNS simulation will allow for much more accurate solutions of the wake stability because the actual wake behind a self propelled object can be obtained, and much more accurate responses of the wake to perturbations.

Bibliography

[1] YD Afanasyev. Wakes behind towed and self-propelled bodies: asymptotic theory. *Physics of Fluids*, 16:3235, 2004.

[2] C.M. Bender and S.A. Orszag. *Advanced Mathematical Methods for Scientists and Engineers I: Asymptotic Methods and Perturbation Theory*. Advanced Mathematical Methods for Scientists and Engineers. Springer, 1999.

[3] C.G. Canuto, Y. Hussaini, A. Quarteroni, and T.A. Zang. *Spectral Methods: Evolution to Complex Geometries and Applications to Fluid Dynamics*. Scientific Computation. Springer, 2007.

[4] S.C. Chapra. *Applied numerical methods with MATLAB for engineers and scientists*. McGraw-Hill Higher Education, 2008.

[5] W.O. Criminale, T.L. Jackson, and R.D. Joslin. *Theory and Computation of Hydrodynamic Stability*. Cambridge Monographs on Mechanics. Cambridge University Press, 2003.

[6] P.G. Drazin. *Introduction to Hydrodynamic Stability*. Cambridge Texts in Applied Mathematics. Cambridge University Press, 2002.

[7] PG Drazin and LN Howard. *Hydrodynamic stability of parallel flow of inviscid fluid*. Academic Press New York, 1966.

[8] P.G. Drazin and W.H. Reid. *Hydrodynamic Stability*. Cambridge Mathematical Library. Cambridge University Press, 2004.

[9] Chester E Grosch and Steven A Orszag. Numerical solution of problems in unbounded regions: Coordinate transforms. *Journal of Computational Physics*, 25(3):273 – 295, 1977.

[10] P. Huerre and PA Monkewitz. Absolute and convective instabilities in free shear layers. *Journal of Fluid Mechanics*, 159(1):151–168, 1985.

[11] P. Huerre and P.A. Monkewitz. Local and global instabilities in spatially developing flows. *Annual Review of Fluid Mechanics*, 22(1):473–537, 1990.

[12] L.S. Hultgren and A.K. Aggarwal. Absolute instability of the gaussian wake profile. *Physics of Fluids*, 30:3383, 1987.

[13] D.R. Kincaid and E.W. Cheney. *Numerical Analysis: Mathematics of Scientific Computing*. Pure and applied undergraduate texts. American Mathematical Society, 2002.

[14] MJ Maghrebi. Orr sommerfeld solver using mapped finite difference scheme for plane wake flow. *Journal of Aerospace Science and Technology*, 2(4):55–63, 2005.

[15] A. Michalke. On the inviscid instability of the hyperbolictangent velocity profile. *Journal of Fluid Mechanics*, 19(04):543–556, 1964.

[16] M. Miklavčič. Eigenvalues of the orr-sommerfeld equation in an unbounded domain. *Archive for rational mechanics and analysis*, 83(3):221–228, 1983.

[17] S.A. Orszag. Accurate solution of the orr-sommerfeld stability equation. *J. Fluid Mech*, 50(4):689–703, 1971.

[18] P.J. Schmid and D.S. Henningson. *Stability and Transition in Shear Flows*. Number v. 142 in Applied Mathematical Sciences. Springer, 2001.

[19] SA Smirnov and SI Voropayev. On the asymptotic theory of momentum/zero-momentum wakes. *Physics Letters A*, 307(2-3):148–153, 2003.

[20] D.S. Watkins. *Fundamentals of Matrix Computations*. Pure and Applied Mathematics. John Wiley & Sons, 2002.

[21] JA Weideman and SC Reddy. A matlab differentiation matrix suite. *ACM Transactions on Mathematical Software (TOMS)*, 26(4):465–519, 2000.